Authors' response to reviewers

We are grateful to both reviewers for their detailed and constructive comments which have greatly improved the manuscript. We provide a response to the general comments and then specific comments of each reviewer below. All of the resulting changes are included in the track changes version of the manuscript, provided as an appendix to this response. The new corresponding line numbers are also indicated in the response to each comment.

General Comments, Reviewer 1

[1] Most (all?) of the conclusions could have been found in previous studies.

We do not agree with this statement, particularly as the precipitation results from a number of the studies have not previously been published (Section 2) and none of the simulations described have been compared to quantitative precipitation proxies. Our study contains several new insights into the hydrology of the Eocene, including both model-data comparisons and model intercomparison.

(i) Model-data comparisons. The majority of sites for which we show proxy-model comparisons in this paper have not been compared quantitatively to GCM data in the published literature. A low precipitation bias for the Canadian Arctic is described by Greenwood et al. (2010) where their proxy estimates are suggested to be 2-4x model-derived values. The comparison presented in our paper provides a more systematic exploration of proxy-model anomalies and shows that a low precipitation model bias is reproducible across a number of high-latitude sites including elsewhere within the Arctic, the Antarctic and southern Australia (Figure 10). This is important both because precipitation is spatially discontinuous (and more so than temperature) - and because error bars on precipitation proxies are currently unavoidably large. That the bias is reproduced at a number of sites suggests this is more likely to be a robust data-model anomaly.

As we note on lines 568 - 570, a precipitation model-data comparison was undertaken by Speelman et al. (2010) for the Eocene Azolla interval (~49 Ma), but this was an atmosphere-only simulation, run with Eocene proxy-inferred SSTs i.e. an imposed low tropical-pole temperature gradient. Whilst that study concluded that the good match between GCM output and both precipitation estimates and water isotopes supported a low Eocene temperature gradient, a range of proxy data were omitted from their analysis or have been published since (lines 571 - 574), which greatly extends the spatial coverage, including at high latitudes.

(ii) Model inter-comparison. There has previously been no GCM inter-comparison or assessment of structural uncertainty arising from differing model physics, parameterisation schemes and boundary conditions, like there has been for temperature (lines 122 - 126). Future climate predictions, such as those shown in the IPCC reports, have shown a divergence in the response of the hydrological cycle between GCMs, and so developing an understanding of model spread for past warm periods is arguably an important step towards evaluating GCM performance. We have shown that model differences are particularly important for the Eocene over tropical regions, over peri-Tethys (Figures 3, 5 and 6) and the South Pacific region (Figures 5 and 10). Our new Figure 12 summarises where the greatest model-data mismatches are found.

Our paper is the first to compare the hydrological cycle simulated across coupled GCMs for the Eocene; much work remains to be done in fully characterising the response, but we hope this work will provide a foundation for future work. Even if the coupled temperature-precipitation relationship we describe (Figure 11) is somewhat intuitive, its demonstration is important for understanding Eocene paleoclimate: it provides independent evidence that model-simulated climatology is problematic at high latitudes.

[2] The utility of models is that they can be probed to understand the reason for the solutions that they give… this study provides very little insight into the mechanisms responsible for the model differences it describes.

We agree on the utility of models, but to robustly explain the range of hydrological behaviour would require common experimental design between all simulations, and/or a number of additional sensitivity studies. As we explain in lines 132 - 139 the models differ in a number of boundary conditions and show some substantial differences in their simulation for preindustrial climate (Figure 1), where boundary conditions are largely constant. Any Eocene differences are therefore both the result of differences in boundary conditions and model physics. Some of the models with multiple simulations at different atmospheric CO_2 levels hint at underlying mechanisms, however, the FAMOUS simulations, performed at 2 x CO_2, indicate that a range of behaviour is possible within a single model arising from parametric uncertainty alone (Figure 2). Furthermore a number of the GCMs have only single Eocene simulations (ECHAM5, GISS-ER), which limits our ability to fully explain responses. Following comments 18, 20, 22 and 23, we have also added some further explanations to the paper.

We agree that there is clearly a need to develop a greater mechanistic understanding behind some of the differences which our paper has highlighted. Such intercomparisons will be facilitated in the near future via the 'DeepMIP' project - a deep time model intercomparison project*. This will promote common experimental designs across modelling groups for deep-time high-CO_2 climate states including the Eocene, in a similar way to the PMIP framework has done for the Mid-Pliocene, Last Interglacial, Last Glacial Maximum and Mid-Holocene. In the meantime, this work aims to understand the differences as best we can in the context of the simulations available.

* http://gtr.rcuk.ac.uk/projects?ref=NE/N006828/1

[3] Greenhouse gases other than CO2 are generally not stated, nor are orbital parameters.

In the case of greenhouse gases, where not stated, this is because they are held at preindustrial levels, which we have now made clearer in the manuscript (line 145). Where varied, we have stated this in Section 2, and estimated the net forcing in terms of CO_2 equivalent. We have now included orbital parameters in Table 1. Note that some of the simulations within the ensemble adopt a preindustrial orbital configuration, whilst others utilise an idealised Eocene orbital configuration, although many configurations would have been possible during the sustained warmth of the Early Eocene Climatic Optimum (EECO). Understanding whether there are regional effects of these orbital difference on precipitation distribution would require further simulations (see comment 2).

[4] Differences in geography are also not described, which may be appropriate, since the paleographies appear similar. Topography may be a different issue, though, and should be shown. What is the mean continental land elevation? To what degree can differences in topography account for regional hydrological changes?

The sources of the paleogeographic reconstructions used in each simulation are summarised in Table 1. The effect of topography is a good point, particularly as improvements in the simulation of precipitation distribution in modern-day climate simulations often come about through better resolved topography. However, there does not appear to be a strong relationship between orography and precipitation distribution. We have now included an additional supplementary figure (Fig S5) which shows differences in precipitation rate and topography between three pairs of simulations which have a similar global precipitation rate. We have added a paragraph to the manuscript which discusses this figure and explains that there is not a strong relationship between differences in orography and precipitation rate between the models (lines 437 - 449).

[5] The models also have very coarse resolution, which is well known to degrade the simulation of precipitation. Some discussion of this is warranted as well. Is there any connection between atmospheric model resolution and precipitation sensitivity or response?

This is a good point, and we have added a statement to the conclusion regarding the need to analyse the precipitation response in higher resolution models (lines 662 - 666). We assume here that the reviewer is referring to precipitation sensitivity in terms of dp/dT responses shown in Figure 2. Although the models differ in their atmospheric grid resolution (Table 1), they do not span a sufficient range of resolution to assess the effect, particularly as the highest resolution model, HadCM3L has a similar dp/dT sensitivity to CCSM3. The slightly lower resolution GISS-ER has only a single Paleogene simulation. However, FAMOUS is notably lower resolution than the other models and was shown to have a different precipitation sensitivity (Figure 2) and we agree that this is an area which could be investigated in future via high-resolution Eocene simulations. In terms of the spatial patterns of precipitation, high-resolution atmosphere-only simulations (T170 grid; 0.7 ° latitude x 0.7 ° longitude) have been performed by co-author Matt Huber, with SSTs specified from coupled runs (CCSM3_H). The precipitation patterns are qualitatively the same as those we show here, and so we expect model-data biases to not be significantly improved.

[6] In general, the paper could use editing and streamlining. It's too long and rambles in parts.

We have aimed to tighten up the language and streamline the paper where possible. All editorial changes are shown on the track changes version of the manuscript.

Specific Comments: Reviewer 1

[7] Title. Change the title. I suggest "Comparison of the early Eocene hydrological. . ."

We have changed the title to: *'A model-model and data-model comparison for the early Eocene hydrological cycle'*.

[8] Abstract, line 15. "This is primarily due to elevated atmospheric paleo-CO2." As shown in the manuscript, this is due to elevated temperatures.

This has been clarified (line 33).

[9] p. 3281, lines 1, 6, etc. Surface surface temperature and mean annual temperature are not proper names and should be not capitalized.

Corrections have been made throughout the manuscript.

[10] p. 3281, line 26-28. "This has resulted in suggestions. . ." This is an incomplete sentence. Please fix.

This sentence has been clarified (lines 86 - 90).

[11] p. 3289, lines 12-14. What are the sources of these biases? Are they a concern for simulating the Eocene?

These are a concern for the Eocene and part of the reason of showing how well the models perform for the preindustrial is to demonstrate that even with good knowledge of boundary conditions, all GCMs are liable to produce errors in their precipitation distribution (Sect 3.1). Although similar preindustrial distributions have been shown previously (e.g. IPCC model evaluation chapters), we show these here to contextualise our Eocene observations (see manuscript Sect 3.3.1). We have added some further references to the manuscript which discuss the sources of these biases (lines 248, 252 - 253).

[12] p. 3289. Fig. S1. This figure should be moved to the main text, as it more clearly shows extratropical model skill in simulating precipitation than absolute precipitation anomalies. Also, please include the relative anomalies for the ocean as well. Some explanation should be added to explain the very large relative biases that show up over the continents.

We have added anomalies over the oceans to Fig. S1, but have retained this within the Supplementary Information. The reason for this is that our proxy-model comparisons (Figures 10 – 11) show rates and anomalies in mm/day, which can more easily be related to the existing Figure 1. We have added some further references to the manuscript which discuss the sources of continental biases (line numbers 252 – 253; 263 – 264).

[13] p. 3290, lines 3-5. "EoMIP models simulate a global precipitation rate which agrees fairly well with observational data sets" I agree that this is the case. But, mean annual precipitation is not a good measure of model skill for the obvious reason that cancellation of large biases can make a poor model appear skillful (e.g Fig. 1 of this paper). Mean annual precipitation shouldn't be the determinant for whether to use a model or not.

We have removed this sentence, but retain the observational data for information purposes. Since we evaluate precipitation sensitivity in terms of global precipitation rate (Figure 2), this is a useful confirmation that there is some physical basis to the model estimated rate.

[14] p. 3290, lines 23-25. ". . .consider mean annual precipitation to be a robust estimate of the overall sensitivity. . ." This may well be the case, however the authors' justification for this, that the interannual variability in global average precipitation is small, is not evidence that this is the case.

We have now removed this sentence.

[15] p. 3290, lines 24-27. This sentence indicates that the authors determined that the observational datasets could be used because they compare well with the model results. I assume that the authors did not intend this meaning.

We have now corrected this sentence (line number 285 - 286).

[16] p. 3291, lines 6-10. The authors promise here to discuss four reasons for differences in global precipitation rates between models. There is considerable discussion of the role of temperature, but almost none of these other factors. Please add this discussion.

Our original intention was not to indicate that temperature operated independently of the other controls and so we have rephrased this section (line numbers 292 - 294). As we show, differences in Eocene boundary conditions – which includes atmospheric CO_2 and variation of poorly constrained parameters – such as the cloud condensation nuclei or aerosol loading – often impact the global precipitation rate via a mediating effect on temperature.

[17] p. 3292, lines 20-24. "may relate to more fundamental differences in model physics" Okay. Please explain and demonstrate what these are.

We have clarified our reasoning (line 324 - 329), but note that further simulations with equivalent parameterisation schemes for large-scale and convective precipitation would be required to confirm this hypothesis.

[18] p. 3293, lines 2-3. The authors need to demonstrate that moisture availability is the reason for the reduced sensitivity. They could do this in a number of ways, e.g. by quantifying changes in continental moist availability or continental relative humidity.

We have included an additional supplementary figure (Fig. S3) and added discussion on lines 337 - 339.

[19] p. 3294, lines 5-6. "Paleogene boundary conditions other than CO2 are crucial in elevation precipitation rate in this model." Why? How exactly? This point is interesting because it contradicts the conclusions from the HadCM3L model (p. 3293, lines 18-20). Why are these models responding differently to Paleogene boundary conditions?

We have added some explanation to line 363 - 365.

[20] p. 3295, lines 8-9. "The SPCZ is CCSM is also far weaker in the Eocene simulations. . ." Why?

We have included an additional supplementary figure (Fig. S4) and added discussion on lines 387 - 392.

[21] p. 3295, lines 9-11. ". . .CCSM and HadCM3L strongly diverge in the Eocene. . ." Why?

We have added discussion on lines 394 - 395.

[22] p. 3295, lines 19-20, Fig. 5. It's not clear why the authors have selected the models in the way that they have, on the basis of a "common global precipitation rate". Results from all the models could be shown by using anomalies from the global average rather than absolute values.

The problem in producing a multi-model mean is that there is no CO_2-forcing common across all models. Furthermore, even where a number of model do have a common-CO_2 forcing, differences in parameterisation schemes (particularly in the case of FAMOUS simulations and CCSM3_K) would result in taking a mean across simulations with substantially different amounts of water vapour in the atmopshere and global precipitation rates. Instead, we have chosen simulations which display a near common global precipitation/evaporation rate (or have interpolated between simulations assuming linear responses – see caption for Figure 6). This means that our multimodel mean provides an indication of how much regional variability exists in precipitation rate between a number of simulations which have same global strength of the hydrological cycle.

There are clearly caveats to this approach (for example, we have included 2 x HadCM3L simulations (Lunt and Loptson) and 2 x CCSM3 simulations (Huber and Winguth), which results in the multimodel mean being biased away from the ECHAM model. We have clarified the manuscript on line 400 - 405 to more clearly explain our reasoning.

[23] p. 3297, lines 10-11. "HadCM3L displays far greater spatial contrasts in net precipitation change.." Why?

We have included an additional supplementary figure (Figure S5) and added discussion on lines 459 - 463.

[24] Section 3.4. The authors should omit this section on monsoons. The topic is not given sufficient attention. The monsoon results are summarized in a single figure without any real explanation of the results.

The seasonality of precipitation is of particular importance in the Eocene with modelling and proxies sometimes producing contrasting results – see e.g. the recently published West et al. (2015). In particular, high latitudes are of interest: some studies have suggested Antarctic (Jacques et al., 2014) and Arctic (Schubert et al., 2012) regions were subject to seasonal precipitation regimes, whereas other work, including the modelling work of Huber and Goldner (2012) have shown more equable, year round precipitation. We believe that analysis is worth retaining in the manuscript as it highlights the difference in seasonality at the high-latitudes. This could be the reason why colder pole models such as HadCM3L display a greater proxy-model anomaly (lines 640 - 641).

[25] p. 3304, lines 1-4. The explanation given doesn't make sense. The failure of the models to predict enough precipitation isn't a result of too much rainout. The precipitation is too low either because there is not sufficient vapor (the saturation pressure is too low) or because not enough of the vapor is undergoing condensation (the lapse rate is too low).

This line has been clarified (line 619).

[26] p. 3304, line 6. "anomalies" should be "differences"

This has been amended to proxy-model differences (line 622).

[27] p. 3304, lines 23-24. I don't understand the point being made here. Please explain more fully.

We have removed this line in our edits to the manuscript.

[28] p. 3336, Fig. 9. The differences in implied latent heat fluxes between models are quite large. In some models, the latent heat flux is symmetrical between hemispheres and in others it is not. Some discussion of these results, and the dynamics behind them, are required.

Some edits have been made to this section and we have explained the reasons for the asymmetry in response on 533 - 539.

[29] Refs. Gasson et al. (2013) is cited but is missing from the references.

The correct citation has now been added to the reference list.

<u>General Comments, Reviewer 2</u>

[30] As the paper is currently laid out, the proxy data are treated together as an estimate of what Eocene precipitation was like, however in reality each proxy estimate provides an independent estimate of what precipitation was like at one point in space and time.

We agree and have made this more explicit in the manuscript (lines 577- 579). In practice, this means that looking at spatial patterns of proxy-model agreement is particularly problematic and so on the whole we avoid such comparisons in favour of the bar charts style plots where comparisons are provided for each data point across a range of CO_2 simultaneously. These span a range of plausible CO_2 including atmospheric concentrations suitable for the mid-Eocene. However, this caveat does mean that comparisons like that of Figure 11 are somewhat biased as they assume the data points can be treated as a group. More extensive and better dated proxies would clearly be beneficial here.

[31] My opinion is that there could be a more complete introduction detailing the climate dynamics that create our expectation of hydrologic intensification in warmer climates.

We have added some additional background to the introduction of the manuscript on lines 110 - 116.

[32] P 3299 Line 12: Should the partition of runoff and groundwater not also depend on how vegetation is parameterized in the various models?

We agree and have amended this sentence to reflect this (line 505).

[33] Line 17: "the wet become wetter and the dry become drier" seems like useful background for what's generally expected in warmer climates, so perhaps belongs in the introduction.

We have made some edits here, and this has additionally been added to the introduction (lines 110 - 116).

[34] P3300: The discussion of the differing response of meridional heat transport would benefit from more explanation of the role of such transport in the global heat budget. If one model produces more latitudinal heat transport (by latent heat of water vapor) than another, does that mean that it must necessarily feature less meridional heat transport via sensible atmospheric and ocean heat? Or, do the differing effects of pCO2 on the surface radiative heat budget at different latitudes mean that different models are allowed to have different total meridional heat transport for given levels of pCO2?

We have made some edits to this section of the manuscript along the lines of comments from Reviewer 1 (lines 533 - 539), but we note that the meridional heat transport is not constrained to be the same within the models. Although they have broadly similar solar radiation at the top of the atmosphere, differing amounts of heat transport and ocean heat transport occur within the models, giving rise to different temperature gradients (e.g. see Lunt et al., 2012).

[35] P3301 Line 10: "They" should be "these" or "the"

This sentence has been corrected (line 554).

[36] Table 3: Clarify what "MA" means here.

Table 3 has been clarified.

[37] Figure 9: It would be nice to see the modern real-world P-E and inferred heat transport to compare to the model control cases.

This is challenging, since observational precipitation and evaporation data are not constrained to be in equilibrium. For example, one such data source which contains both P and E is the ECMWF ERA reanalysis data (Dee et al., 2011). This yields a global precipitation rate of ~2.96 mm/day (c.f. Figure 2) and evaporation of ~2.84 mm/day. Because of this imbalance, the implied northwards flux does not balance to zero and as such there appears to be a net loss of energy from the system via latent heat. We have, however, added the P – E distribution of the ERA 40 data to Figure 8. The most noticeable difference to the HadCM3L preindustrial distribution is the far stronger net-precipitation zone associated with the ITCZ, whilst the differences in location of the net-precipitation and net-evaporation zones is fairly minimal. However, we note that the tropical latitudinal maximum in the ERA-40 data is > 50 cm/year a greater than that in the CMAP data. All of the observational data have their own biases, which we have not considered in this paper.

[38] Figure 10: Give age ranges for each of the sources of proxy data. This is certainly a complicating factor in model-data comparison: many of these data come from different time periods with different climates. Do any of them come from within the PETM or other hyperthermals? This would be especially troublesome.

We have added the age ranges from Table S3 to the captions on each subfigure. Note that these vary in their precision according to the original reference dating. The spread in age is certainly a complicating factor (also see reply to comment 30) and we agree that it is important this should be explicit within the manuscript. None of the data within Figure 10 are specifically dated to any of the hyperthermals with the exception of a possible PETM-age for the Otaio Gorge (New Zealand) data sample of Pancost et al. (2013), now noted in the text (line 575).

Editor's Comment

[39] Assuming that reviews are generally positive, I think there very much should be a new figure 1 that gives a tectonic map of the early Eocene world that shows locations which presently have (perhaps) relevant observations, and maybe regions (shaded) which indicate areas of maximum interest to test modeling.

We agree with this suggestion, but rather than an introductory figure, we have used this suggestion as a concluding figure, which is a useful way of highlighting that some of the regions of greatest model spread occur where there is currently a lack of quantitative precipitation estimates for the early-mid Eocene (Figure 12).

A model-model and data-model comparison for the early Eocene hydrological cycle

~~Insights into the early Eocene hydrological cycle from an ensemble of atmosphere–ocean GCM simulations~~

M. J. Carmichael[1,2], D. J. Lunt[1], M. Huber[3], M. Heinemann[4], J. Kiehl[5], A. LeGrande[6], C. A. Loptson[1], C. D. Roberts[7], N. Sagoo[1,a], C. Shields[5], P. J. Valdes[1], A. Winguth[8], C. Winguth[8], and R. D. Pancost[2]

[1]BRIDGE, School of Geographical Sciences and Cabot Institute, University of Bristol, UK
[2]Organic Geochemistry Unit, School of Chemistry and Cabot Institute, University of Bristol, UK
[3]Climate Dynamics Prediction Laboratory, Department of Earth Sciences, The University of New Hampshire, USA
[4]~~International Pacific Research Center, School of Ocean and Earth Science and Technology, University of Hawaii, USA~~Institute of Geosciences, Kiel University, Germany
[5]Climate and Global Dynamics Laboratory, UCAR/NCAR, USA
[6]NASA Goddard Institute for Space Studies, USA
[7]The Met Office, UK
[8]Climate Research Group, Department of Earth and Environmental Sciences, University of Texas Arlington, USA
[a]now at: Department of Geology and Geophysics, Yale University, USA

Received: 19 June 2015 – Accepted: 25 June 2015 – Published: 17 July 2015
Correspondence to: M. J. Carmichael (matt.carmichael@bristol.ac.uk)
Published by Copernicus Publications on behalf of the European Geosciences Union.

Abstract

Recent studies, utilising a range of proxies, indicate that a significant perturbation to global hydrology occurred at the Paleocene–Eocene Thermal Maximum (PETM; 56 Ma). An enhanced hydrological cycle for the warm early Eocene is also suggested to have played a key role in maintaining high-latitude warmth during this interval. However, comparisons of proxy data to General Circulation Model (GCM) simulated hydrology are limited and inter-model variability remains poorly characterised, despite significant differences in simulated surface temperatures. In this work, we undertake an intercomparison of GCM-derived precipitation and $P-E$ distributions within the extended EoMIP ensemble (Lunt et al., 2012), which includes previously-published early Eocene simulations performed using five GCMs differing in boundary conditions, model structure and precipitation relevant parameterisation schemes.

We show that an intensified hydrological cycle, manifested in enhanced global precipitation and evaporation rates, is simulated for all Eocene simulations relative to preindustrial. This is primarily due to elevated atmospheric paleo-CO_2, resulting in elevated temperatures, although the effects of differences in paleogeography/ice sheets are also of importance in some models. For a given CO_2 level, globally-averaged precipitation rates vary widely between models, largely arising from different simulated surface air temperatures. Models with a similar global sensitivity of precipitation rate to temperature (dP/dT) display different regional precipitation responses for a given temperature change. Regions that are particularly sensitive to model choice include the South Pacific, tropical Africa and the Peri-Tethys, which may represent targets for future proxy acquisition.

A comparison of early and middle Eocene leaf-fossil-derived precipitation estimates with the GCM output illustrates that a number of GCMs underestimate precipitation rates at high latitudes. Models which warm these regions, either via elevated CO_2 or by varying poorly constrained model parameter values, are most successful in simulating a match with geologic data. Further data from low-latitude regions and better constraints on early Eocene CO_2 are now required to discriminate between these model simulations given the large error bars on paleoprecipitation estimates. Given the clear differences ~~apparent~~ between simulated precipitation distributions within the ensemble, our results suggest that paleohydrological data offer an independent means by which to evaluate model skill for warm climates.

1 Introduction

Considerable uncertainty exists in understanding how the Earth's hydrological cycle will function on a future warmer-than-present planet. State-of-the-art General Circulation Models (GCMs) show a wide inter-model spread for future precipitation and runoff responses when prescribed with the same greenhouse gas emission trajectories (IPCC, 2013; Knutti and Sedlácek, 2012). Remarkably few studies have investigated the hydrology of ancient greenhouse climates, but understanding how the hydrological cycle operated differently during these intervals could provide insight into the mechanisms which will govern future changes and the sensitivity of these processes (e.g. Pierrehumbert, 2002; Suarez et al., 2009; White et al., 2001). In particular, characterising the hydrological cycle simulated in GCMs using paleo-boundary conditions and comparisons to geological proxy data can contribute to developing an understanding of how well models that are used to make future predictions perform for warm climates.

The early Eocene (56–49 Ma) represents the warmest sustained interval of the Cenozoic, with evidence for substantially elevated global temperatures relative to modern in both marine (Zachos et al., 2008; Dunkley Jones et al., 2013; Inglis et al., 2015) and terrestrial settings (Huber and Caballero, 2011; Pancost et al., 2013). This is particularly evident at high latitudes: pollen and macrofossil evidence indicate near-tropical forest growth on Antarctica during the Early Eocene Climatic Optimum (EECO; Pross et al., 2012; Francis et al., 2008) and fossils of fauna including alligators, tapirs and non-marine turtles occur in the Canadian Arctic (Markwick, 1998; Eberle, 2005; Eberle and Greenwood, 2012). Absolute temperatures for the Paleogene remain controversial (e.g. Taylor et al., 2013; Douglas et al., 2014; Hollis et al., 2012), but quantitative estimates from multiple proxies support substantial global warmth. Mean annual s~~S~~ea s~~S~~urface t~~T~~emperature (SST) for the Arctic has been estimated at ~ 17–18 °C rising to ~ 23 °C during the Paleocene–Eocene Thermal Maximum (PETM) hyperthermal at 56Ma (TEX86'; Sluijs et al., 2006). SSTs may have reached 26–28 °C in the Southwest Pacific during the Early Eocene Climatic Optimum (EECO, TEX^{L}_{86}; Hollis et al., 2012; Bijl et al., 2009). EECO ~~Mean~~ mean annual a~~A~~ir t~~T~~emperature (MAT) of Wilkes' Land margin on Antarctica has been estimated at 16±5 °C (Nearest Living Relative, NLR, based on paratropical vegetation), with summer temperatures as high as 24–27 °C, inferred from soil bacterial tetraether lipids (MBT/CBT; Pross et al., 2012); similar but slightly higher MATs were obtained from New Zealand (Pancost et al., 2013). ~~Low~~ Low-latitude data are scarce, but oxygen isotopes of planktic foraminfera and TEX_{86} indicate SSTs off the coast of Tanzania > 30 °C (Pearson et al., 2007; Huber, 2008).

Few proxy estimates of early Eocene atmospheric carbon dioxide exist. Paleosol geochemistry indicates concentrations could have reached ~ 3000 ppmv (Yapp, 2004; Lowenstein and Demicco, 2006), whilst stomatal index approaches yield more modest values of 400–600 ppmv (Royer et al., 2001; Smith et al., 2010). Recent modelling indicates that terrestrial methane emissions also could have been significantly greater than modern, representing an additional greenhouse gas forcing (Beerling et al., 2011). GCM simulations with greenhouse gas concentrations substantially elevated compared to modern have had greatest success in reproducing proxy-inferred warmth (Huber and Caballero, 2011; Lunt et al., 2012), providing further evidence that global Eocene warmth was maintained by elevated concentrations of greenhouse gases. However, simulating warm ~~high-~~ high-latitude and equable continental interior temperatures remains a challenge, with models struggling to replicate the reduced equator-pole temperature gradient implied by the proxies (Huber and Sloan, 2001; Valdes, 2011; Pagani et al., 2013 and references therein). ~~This has resulted in suggestions that GCMs may be missing key heat transfer processes, new modelling aimed at reducing data-model anomalies, as well as re-evaluations of existing proxy data~~ This has resulted in the suggestion that GCMs may be missing key heat transfer processes or mechanisms for warmth (e.g. Abbot and Tziperman, 2008; Huber et al., 2004; Korty et al., 2002; Kirk-Davidoff et al., 2002), as well as re-evaluation of existing proxy data and new modelling aimed at reducing data-model anomalies (Sagoo et al., 2013; Kiehl and Shields, 2013; Loptson et al., 2014; Sluijs et al., 2006; Huber and Caballero, 2011; Lunt et al., 2012).

The hydrology of this super-greenhouse climate state remains poorly characterised. Initial observations of globally widespread Eocene laterites and coals (Frakes, 1979; Sloan et al., 1992) and of enhanced sedimentation rates and elevated kaolinite in the clay fraction of many coastal sections (Bolle et al., 2000; Bolle and Adatte, 2001; John et al., 2012; Robert and Kennett, 1994; Nicolo et al., 2007) suggested early Eocene terrestrial environments were characterised by globally enhanced precipitation and runoff relative to today. Diverse geochemical proxies are now providing a more nuanced interpretation of how the spatial organisation of the Eocene hydrological cycle differed from that of the modern. This is particularly the case for the PETM. In the Arctic, the hydrogen isotopic composition of putative leaf-wax compounds is enriched by ~ 55‰ δD at the PETM, thought to reflect increased export of moisture from low latitudes (Pagani et al., 2006). Enrichment of δD in leaf waxes from tropical Tanzania, coincident with elevated concentrations of terrestrial biomarkers and sedimentation rates, has been interpreted as indicating a shift to a more arid climate with seasonally heavy rainfall (Handley et al., 2012, 2008). Whether these changes are typical of the low latitudes or are highly localised responses remains to be determined. Elsewhere, conflicting evidence for regional hydrological changes exist: an increased PETM offset in the magnitude of the Carbon Isotope Exursion (CIE) between marine and terrestrially derived carbonates, including from Wyoming, has been suggested to reflect increases in humidity/soil moisture of the order of 20–25% (Bowen et al., 2004). Other studies utilising leaf physiogonomy and paleosols suggest the North American continental interior became drier at the onset of the PETM, or alternated between wet and dry phases (Kraus et al., 2013; Smith et al., 2007; Wing et al., 2005).

Modelling studies have suggested future warm climates will be characterised by an exacerbated *P - E* distribution – broadly ~~where~~resulting in wet climates becomes wetter and ~~the~~ dry becomeing drier, which arises from increased water vapour transport into moisture convergence zones from moisture divergence zones (Held and Soden, 2006; Chou and Neelin, 2004). An intensified hydrological cycle, associated with increased meridional transport of water vapour is therefore consistent with regions of both wetting and drying. However, this thermodynamic response may be complicated by dynamical shifts in atmospheric circulation (e.g. Chou et al., 2009; Bony et al., 2013; Chadwick et al., 2013). Despite this framework for understanding warm climate hydrological responses and ~~these~~ proxy indications of an ~~background~~ early Eocene hydrological cycle different to modern, ~~and of significant hydrological changes at the PETM,~~ only limited proxy-model comparisons have been made for the early Eocene hydrological cycle (Pagani et al., 2006; Speelman et al., 2010; Winguth et al., 2010). Some analysis of model sensitivity of precipitation and $P - E$ to imposed CO_2 (Winguth et al., 2010), paleogeography (e.g. Roberts et al., 2009) and parametric uncertainty (Sagoo et al., 2013; Kiehl and Shields, 2013) has been undertaken, but the range of hydrological behaviour simulated within different models has not yet been assessed. Lunt et al. (2012) undertook a model intercomparison of early Eocene warmth, EoMIP, based on an ensemble of 12 Eocene simulations undertaken in four fully-coupled atmosphere–ocean climate models, a summary of which is given in Table 1. This demonstrated differences in global surface air temperature of up to 9 °C for a single imposed CO_2 and differing regions of CO_2-induced warming, but the implications for the hydrological cycle have not been considered.

This study addresses three main questions: (1) how do globally averaged GCM precipitation rates for the Eocene compare to preindustrial simulations and vary between models in the EoMIP ensemble? (2) How consistently do the EoMIP GCMs simulate regional precipitation and $P - E$ distributions? (3) Do differences between models affect the degree of match with existing proxy estimates for mean annual precipitation?

2 Model descriptions

The EoMIP approach of Lunt et al. (2012) is distinct from formal model intercomparison projects which utilise a common experimental design (e.g. PMIP3, Taylor et al., 2012; CMIP5, Braconnot et al., 2012). Instead, the EoMIP models differ in their boundary conditions and span a plausible early Eocene CO_2 range, utilise different paleogeographic reconstructions and specify different vegetation distributions. This is in addition to internal differences in model structure and physics, including precipitation-relevant parameterisations such as those relating to convection and cloud microstructure. Whilst this may hinder the identification of reasons for inter-model differences, the ensemble spans more fully the uncertainty in boundary conditions, which is appropriate for deep time climates such as the early Eocene.

The ensemble, summarised in Table 1, includes a range of published simulations of the early Eocene carried out with fully dynamic atmosphere–ocean GCMs. We extend the EoMIP ensemble as originally described by Lunt et al. (2012) to include simulations published by Sagoo et al. (2013), Kiehl and Shields (2013) and Loptson et al. (2014). A brief description of each model and the corresponding simulation is given below. Each model produces large-scale (stratiform) and convective precipitation separately, also summarised in Table 1. Greenhouse gases other than CO_2 are only varied in some of the simulations and are held at preindustrial levels in a number of the models; we have therefore estimated the forcing in terms of net CO_2 equivalent, detailed below.

2.1 HadCM3L

HadCM3L is a version of the GCM developed by the UK Met Office (Cox et al., 2000). Eocene simulations performed with atmospheric CO_2 at ×2, ×4 and ×6 preindustrial levels were presented by Lunt et al. (2010) in their study of the role of ocean circulation as a possible PETM trigger via methane hydrate destabilisation. In these simulations, models were integrated for more than 3400 years to allow intermediate-depth ocean temperatures to equilibrate. Both the atmosphere and ocean are discretised on a 3.75° longitude × 2.5° latitude grid, with 19 vertical levels in the atmosphere and 20 in the ocean. Vegetation is set to a globally homogenous shrubland.

The effect of using an interactive vegetation model, TRIFFID (Cox, 2001), on temperature proxy-model anomalies was considered by Loptson et al. (2014) who performed simulations at ×2 and ×4 CO_2, continuations of those of Lunt et al. (2010). This study indicated that for a given prescribed CO_2, the inclusion of dynamic vegetation acts to warm global climate via albedo and water vapour feedbacks. We refer to these simulations as HadCM3L_T. The effect of dynamic vegetation on precipitation distributions and global precipitation rate was additionally briefly considered but comparisons to precipitation proxy data or to other models have not been undertaken.

2.2 FAMOUS

FAMOUS is an alternative version of the UK Met Office's GCM, adopting the same climate parameterisations as HadCM3L, but solved at a reduced spatial and temporal resolution in the atmosphere (Jones et al., 2005; Smith et al., 2008). Atmospheric resolution is 7.5 ° longitude × 5 ° latitude, with 11 levels in the vertical, whilst the ocean resolution matches that of HadCM3L. Both modules operate at an hourly time-step. Because of its reduced resolution, FAMOUS has been used for transient simulations with long run-times and in perturbed parameter ensembles where a large number of simulations are required (Smith and Gregory, 2012; Williams et al., 2013). Sagoo et al. (2013) used FAMOUS to study the effect of parametric uncertainty on early Eocene temperature distributions by varying 10 climatic parameters which are typically poorly constrained in climate models. Their results demonstrated that a globally warm climate with a reduced equator-to-pole temperature gradient can be achieved at 2 × preindustrial CO_2. Of the seventeen successful simulations which ran to completion, our focus is on E16 and E17, the simulations with the shallowest equator-to-pole temperature gradient and which show the optimal match to marine and terrestrial temperature proxy-data. At the ocean grid resolution, the paleogeography matches that of Lunt et al. (2010). Vegetation is set to a homogenous shrubland. All simulations were run for a minimum of 8000 model years and full details of the perturbed parameters are provided in Sagoo et al. (2013). Sagoo et al. show DJF and JJA precipitation distributions for their globally warmest and coolest simulations, but comparisons to other models or to proxy data have not been made.

2.3 CCSM3

We utilise three sets of simulations performed with CCSM3, a GCM developed by the US National Centre for Atmospheric Research in collaboration with the university community (Collins et al., 2006). The first set ~~were~~ was initially used by Liu et al. (2009) in their study of Eocene–Oligocene sea surface temperatures, and subsequently compared to terrestrial proxy data in a study of the early Eocene climate equability problem by Huber and Caballero (2011). These simulations are configured with atmospheric CO_2 at ×2, ×4, ×8 and ×16 preindustrial. Models were integrated for between 2000 and 5000 years, until the sea surface temperature was in equilibrium. The atmosphere is resolved on a 3.75 ° longitude by ~ ° 3.75 latitude (T31) grid with 26 levels in the vertical and the ocean is resolved on an irregularly spaced dipole grid. The prescribed land surface cover follows the reconstructed vegetation distribution utilised in Sewall et al. (2000). Following the approach of Lunt et al. (2012) we refer to these simulations as CCSM3_H.

The second set of simulations, which we refer to as CCSM3_W, ~~were~~ was described by Winguth et al. (2010) and Shellito et al. (2009) and conducted at ×4, ×8 and ×16 preindustrial CO_2. Relative to the CCSM3_H simulations, these simulations utilised a solar constant reduced by 0.44 %, ~~were integrated for a shorter period (_ 1500 years)~~, adopted an updated vegetation distribution (Shellito and Sloan, 2006) and utilised a marginal sea parameterisation, resulting in paleogeographic differences, particularly in polar regions. However, the major difference between the simulations is that the CCSM3_W simulations utilise a modern-day aerosol distribution, whereas CCSM3_H adopts a reduced loading for the early Eocene based on a hypothesised lower early Eocene ocean productivity (Kump and Pollard, 2008; Winguth et al., 2012). However, the extent to which increased volcanism at the PETM might have increased aerosol loading remains uncertain (Svensen et al., 2004; Storey et al., 2007).

The third set of simulations, CCSM3_K, ~~are~~ is described in Kiehl and Shields (2013). This study investigated the sensitivity of Eocene climatology to the parameterisation of aerosol and cloud effects, specifically by altering cloud microphysical parameters including cloud drop number and effective cloud drop radii. Modern day values from pristine regions are applied homogenously across land and ocean. Simulations were performed at two greenhouse gas concentrations corresponding to possible pre- and trans-PETM atmospheric compositions which are equivalent to CO_2 of ~ ×5 and ~ ×9 preindustrial, respectively. Paleogeography and vegetation distribution are the same as those used in CCSM3_W and the solar constant is reduced by 0.487% relative to modern. Changes in precipitation distribution between high- and low-CO_2 simulations have previously been shown for the CCSM3_W and CCSM3_K simulations (Winguth et al., 2010; Kiehl and Shields, 2013), but how robust these Eocene distributions are to GCM choice remains unknown.

2.4 ECHAM5/MPI-OM

The ECHAM5/MPI-OM model is the GCM of the Max Planck Institute for Meteorology (Roeckner et al., 2003), used by Heinemann et al. (2009) in their study of reasons for early Eocene warmth. The model was configured with CO_2 at ×2 preindustrial, using the paleogeography of Bice and Marotzke (2001) and a globally homogenous vegetation cover, with lower albedo but larger leaf area and forest fraction than pre-industrial, equivalent to a modern day woody savannah. Atmosphere components are resolved on a gaussian grid with a spacing of 3.75° longitude and approximately 3.75° latitude. Relative to the preindustrial simulation, methane is increased from 65 to 80 ppb and nitrous oxide from 270 to 288 ppb for the Eocene, but these are negligible relative to change in radiative forcing associated with doubling of preindustrial CO_2. Latitudinal precipitation distributions in the simulation relative to preindustrial were considered by Heinemann et al. (2009) and elevated convective precipitation at high-latitudes suggested to be consistent with convective clouds as a ~~high~~ high-latitude~~s~~ warming mechanism (Abbot and Tziperman, 2008).

2.5 GISS-ER

The E-R version of the Goddard Institute for Space Studies model (GISS-ER; Schmidt et al., 2006) was utilised by Roberts et al. (2009) in their study of the impact of Arctic paleogeography on ~~high~~ high-latitude early Eocene sea surface temperature and salinity. Here, we include the simulation with open Arctic paleogeography of Bice and Marotzke (2001) which is also utilised in the ECHAM5 simulation. The simulation was forced with CO_2 at 4× preindustrial, and CH_4 at 7× preindustrial, equivalent of a total Eocene greenhouse gas forcing of ~ 4.3× preindustrial CO_2. The atmospheric component of GISS-ER has a grid resolution of 4° latitude by 5° longitude with 20 levels in the vertical; the ocean model is of the same horizontal resolution but with 13 levels. Vegetation is prescribed as in Sewall et al. (2000). The hydrological cycle is shown to be intensified for the Paleogene simulation, with elevated global precipitation and evaporation rates, but spatial precipitation distributions were not studied.

3 Results

3.1 Preindustrial simulations

The simulation of precipitation is a particular challenge for GCMs given the range of spatial and temporal scales at which precipitation-producing processes occur, compared to a typical model grid and timestep (e.g. Knutti and Sedlacek, 2013; Hagemann et al., 2006). Model resolution and the parameterisation schemes which account for sub-grid scale precipitation, in addition to temperature distributions, differ between the GCMs in the ensemble (Table 1). We initially summarise model skill in simulating preindustrial m~~M~~ean a~~A~~nnual p~~P~~recipitation (MAP) to provide context for our Eocene model intercomparison and to identify which, if any, precipitation structures are unique to the Eocene, and which are more fundamentally related to errors particular to a given GCM.

Figure 1 shows preindustrial MAP distributions for each GCM in the EoMIP ensemble and anomalies for each preindustrial simulation relative to CMAP observations (Centre for Climate Prediction, Merged Analysis of Precipitation), which incorporates both satellite and gauge data (Yin et al., 2004; Gruber et al., 2000). The following observations can be made:

i. All of the EoMIP GCMs simulate the principal features of the observed preindustrial MAP distribution, although errors occur in their position and strength. The Inter-tropical Convergence Zone (ITCZ), North Atlantic and North Pacific storm ~~s~~tracks and subtropical precipitation minima ~~in~~ over eastern ocean basins are identifiable for each simulation, but differences are evident between the models. Some biases are common to a number of the models, in particular those relating to the ITCZ and tropical precipitation. HadCM3L, FAMOUS, ECHAM5 and CCSM3 all simulate the ITCZ mean annual location north of the Equator, but the South Pacific Convergence Zone (SPCZ) generally extends too far east in the Pacific, and is too zonal, with precipitation equalling that to the north of the Equator to produce a "double-ITCZ" – a common bias in GCMs (Dai, 2006; Lin et al., 2007; Brown et al., 2011~~; Randall et al., 2007~~). The localised rain belt minimum is a result of the Pacific cold-tongue, not present in GISS-ER, which instead simulates a single convergence zone with high mean annual precipitation across the tropics. Other biases which appear common across the ensemble include ~~over-precipitation in the Southern Ocean and~~ too little precipitation over the Amazon (Yin et al., 2013; Joetzer et al. 2013), over-precipitation in the Southern Ocean (Randall et al., 2007 and references therein) and biases in the position of rainfall maxima in the Indo-Pacific (e.g. Liu et al., 2014). ~~and Antarctica (Hack et al., 2006; Randall et al., 2007 and references therein).~~

ii. Errors over the continents are less than those over the oceans. Absolute errors in MAP are largest over the high precipitation tropical and subtropical oceans, and frequently exceed 150 cm year^{-1} in the case of ITCZ and SPCZ offsets. Over the continents, anomalies are generally no greater than 60 cm year^{-1} and more than 80% of the multimodel mean terrestrial surface has an anomaly less than 30 cm year^{-1}. In low precipitation regions, these errors ~~could~~ still result in significant percentage errors (Fig. S1).

iii. Models show regional differences in precipitation skill. Figure 1 demonstrates that some precipitation biases are individual to particular GCMs. Whilst these are most noticeable over the high precipitation tropical and subtropical oceans, such as offsets in the location of maximum precipitation intensity or strength of storm tracks, relative differences within low-precipitation continental regions can also be considerable (Mehran et al., 2014; Phillips and Gleckler, 2006). This is particularly the case for the Sahel region of northern Africa and the Antarctic continental interior (Fig. S2). We hypothesise that GCMs applied to the study of paleoclimates are also likely to show significant regional differences in their precipitation distribution, underlining the importance of model intercomparison. ~~Figure 2 additionally shows that all of the EoMIP models simulate a global precipitation rate which agrees fairly well with observational data sets for preindustrial climatology (CMAP, GPCP, Legates and Willmott, 1990).~~ Given that all of the models simulate the principal features of MAP distribution, we carry all forward to our Eocene analysis. However, it is important to recognise that significant model biases in simulating precipitation distribution exist, even where boundary conditions are well constrained.

3.2 Sensitivity of the global Eocene hydrological cycle to greenhouse gas forcing

The EoMIP model simulations were configured with a range of plausible early Eocene and PETM atmospheric CO_2 levels, yielding a range of global mean surface air temperatures (Lunt et al., 2012). It is therefore possible to evaluate how consistently precipitation rates are simulated across the GCMs (i) for a given CO_2, (ii) for a given global mean temperature, or in the case of those models for which multiple simulations have been performed, (iii) for a given CO_2 change and (iv) for a given global mean temperature change~~.~~ Closure of the GCM global hydrological budget requires that total annual precipitation and evaporation are equal, providing there is no net change in water storage – the imbalances, summarised in Table S1 are < 0.01 mm day^{-1} equivalent. . Mean annual global precipitation rate therefore provides a zero-order indication of the intensity of the global hydrological cycle. ~~In HadCM3L, the interannual range in global annual mean precipitation rate across the 95 years over which mean climatology is averaged is 0.07 and 0.06mmday^{-1} in the ×2 and ×6 CO_2 simulations, respectively, such that the maximum global annual precipitation rate in the timeseries is less than 2.5% above the minimum rate. We therefore consider mean annual precipitation rate to be a robust estimate of the overall sensitivity of the simulated hydrological cycle.~~ Precipitation rates calculated from three modern observational datasets are shown in Fig. 2b (open circles); model-estimated rates derived from preindustrial simulations (filled circles) ~~and~~ are in relatively good agreement with observational data, ~~the rates derived from preindustrial simulations (filled circles),~~ providing confidence in this measure.

All of the EoMIP models exhibit a more ~~intense~~ active hydrological cycle for the Eocene (Fig. 2b; squares) compared to that simulated in the corresponding preindustrial simulations (Fig. 2b; circles). For a given CO_2, the models vary in the intensity of the hydrological cycle they simulate; ~~–~~for example, ECHAM5 has a global precipitation rate at 2 × preindustrial CO_2 comparable to that of CCSM3_W at ~ 12×preindustrial CO_2. In the remainder of this section, we discuss reasons for these differences, which can be attributed to (i) ~~differences in global/regional temperatures between the simulations, (ii)~~ differences in Eocene boundary conditions, including CO_2 (ii~~i~~) variation of poorly constrained parameter values and (iii~~iv~~) more fundamental differences in the ways in which the models simulate hydrology.

The GCMs within the EoMIP ensemble differ in their global mean temperature for a given CO_2 (e.g. Lunt et al., 2012; Fig. 2a). Consequently, the global precipitation rate for each ensemble member is shown in Fig. 2c relative to its globally averaged surface air temperature. This demonstrates that much of the variation between models in precipitation rate arises from these temperature differences. For example, the elevated precipitation rate in the 2×CO_2 ECHAM5 is explained by this model's warmth, being globally > 5 °C warmer than HadCM3L at the same CO_2. Similarly, the enhanced precipitation rate in the CCSM3_K simulations at both ~ ×5 CO_2 and ~ ×9 CO_2 relative to those simulated in CCSM3_H and CCSM3_W are attributable to warmer surface temperatures in CCSM3_K, resulting from alterations to cloud condensation nuclei (CNN) parameters, with a reduction in low-level cloud acting to increase short-wave heating at the surface (Kiehl and Shields, 2013). The reduced aerosol loading in CCSM3_H results in surface warming relative to CCSM3_W (Fig. 2a), which explains much of the 7–8% increase in strength of the hydrological cycle across the CO_2 range studied~~; the ×4 CO_2 simulation in CCSM3_W has approximately the same surface temperature as CCSM3_H at ×2 CO_2.~~ There are effects beyond those induced by surface temperature, however. For example, for a given surface air temperature, the global precipitation rate is consistently weaker in CCSM_W relative to CCSM_H (Fig. 2c) – possibly a result of modified aerosol-cloud interactions due to the changes in prescribed aerosols in CCSM_H.

The degree to which the global hydrological cycle will intensify with future global warming has received much attention (e.g. Allen and Ingram, 2002; Held and Soden, 2006; Trenberth, 2011). Held and Soden (2006) show a ~ 2% increase in global precipitation per degree of warming for AR4 GCMs forced with the A1B emissions scenario, but with notable inter-model variability. For those simulations with multiple CO_2 forcing, it is possible to estimate how this sensitivity varies for the Eocene. We show the dP/dT relationships for each model as well as the increase in % precipitation for a 1 °C temperature increase over the range of 15–30 °C (Table 2). Both CCSM3 and HadCM3L appear to be broadly comparable at ~ 1.8–2.1% increase in the intensity of the hydrological cycle for each degree of warming, consistent with the future climate simulations.

Some variation in the intensity of the hydrological cycle simulated by the EoMIP models may be expected to occur independently of global mean surface air temperature. For preindustrial conditions, boundary conditions are largely constant across the simulations (atmospheric composition, continental positions, orography and ice sheet distribution), yet the simulations show a spread of ~ 0.30 mm day^{-1} – which exceeds the precipitation increase for a doubling of CO_2 from ×2 to ×4 preindustrial in both CCSM3_H (0.13 mm day^{-1}) and HadCM3L (0.18 mm day^{-1}). Differences in global precipitation rate between the preindustrial simulations ~~– these differences~~ are not explained by differences in ~~preindustrial~~ temperature (Fig. 2b) but may relate to more fundamental differences in model physics, particularly between HadCM3L and CCSM3W given that~~,~~ ~~where the~~ a more active hydrological cycle is consistently simulated in HadCM3L for both the Eocene and preindustrial conditions. Further simulations using equivalent precipitation parameterisation schemes for large-scale and convective precipitation would be required to fully evaluate this hypothesis.

For both the ×2 and ×4 CO_2 simulations, the HadCM3L simulations that include the TRIFFID dynamic vegetation model have a near identical precipitation rate to those without (Fig. 2b). However, the ×4 CO_2 simulation with dynamic vegetation is substantially warmer than the ×4 simulation with fixed homogenous shrubland. The inclusion of the dynamic vegetation model acts to warm the surface climate as described in Loptson et al. (2014), but this does not yield an associated increase in precipitation. ~~This may be related to the fact that temperature differences induced by TRIFFID are concentrated over the land surface. N~~ Relative to the fixed shrubland simulations, the TRIFFID simulations show a reduction in continental evapotranspiration in response to doubling of CO_2, which results in diminished moisture availability over the tropical landmass, for a given temperature (Fig S3). The TRIFFID simulations therefore exhibit a reduced hydrological sensitivity of only ~ 1.3% increase in precipitation per degree of warming (dP/dT) compared with ~ 1.8% for the non-TRIFFID simulations.

In the FAMOUS simulations undertaken by Sagoo et al. (2013; Fig. 2d), all simulations are performed at 2×CO_2, but global temperatures range between 12.3 and 31.8 °C on account of simultaneous variation of 10 uncertain parameter values, some of which directly influence cloud formation and precipitation. Within these simulations there is also a linear relationship between surface air temperature and global precipitation (R^2 = 0.965; n = 17) suggesting the global intensity of the hydrological cycle remains primarily coupled to global temperature, despite greater scatter around the dP/dT relationship. Despite this, the overall dP/dT relationship in FAMOUS is higher than that of HadCM3L and HadCM3L+TRIFFID, with a~~n~~ ~ 2.8% increase in precipitation for each degree of warming (Table 2).

In HadCM3L, the 1×CO_2 Eocene and preindustrial simulations have similar global precipitation rates (Fig. 2a), implying that Eocene boundary conditions other than CO_2 do not exert a major influence on the intensity of the hydrological cycle, raising global precipitation rate by only ~ 0.10 mm day^{-1}. ~~However~~Moreover, even this small ~~, this~~ increase is consistent with and likely driven by a small increase in global surface air temperature. Furthermore, the preindustrial simulations for both CCSM3 and HadCM3L lie on, or close to, the Eocene-derived dP/dT lines (Fig. 2c), suggesting that globally, precipitation rate for a given temperature is not increased/decreased for the Eocene, despite differences in low-latitude land–sea distribution, ocean gateways and a lack of Eocene ice sheets. Intriguingly, extrapolating the dP/dCO_2 relationship backwards to 1×CO_2 for CCSM_W would require an Eocene precipitation rate ~

7% above that of the preindustrial rate. This suggests a more substantial effect of Eocene boundary conditions on elevating absolute precipitation rates for CCSM3_W than that seen in HadCM3L, but still operating via temperature effects. GISS-ER has a marginally more vigorous hydrological cycle than the other models for a given global temperature. Roberts et al. (2009) show that the global precipitation rate in a preindustrial 4×CO_2 simulation in GISS-ER is ~ 4% greater than that of the preindustrial, whereas the Paleogene simulation has a precipitation rate ~ 23% above that of the preindustrial. Therefore non-greenhouse gas Paleogene boundary conditions ~~other than CO_2~~ are crucial in elevating precipitation rate in this model~~.~~, in contrast to HadCM3L. However, this also appears to be mediated by temperature effects, given that the Eocene simulations of Roberts et al. (2009) are also substantially warmer than preindustrial geography simulations with 4 x CO_2 greenhouse gas concentrations.

3.3 Variability in m~~M~~ean a~~A~~nnual p~~P~~recipitation (MAP) distribution

3.3.1 Spatial distribution of MAP

Figure 3 shows MAP distributions for each EoMIP simulation. Eocene distributions are relatively similar to those for preindustrial conditions (Fig. 1), with clearly recognisable inter-tropical convergence zone (ITCZ~~),~~)and South Pacific convergence zone (SPCZ) structures, and subtropical precipitation minima, the distributions of which appear to be longstanding characteristics of Cenozoic precipitation. Relative to preindustrial simulations, the Eocene distributions exhibit increased precipitation at high latitudes as a consequence of elevated ~~Eocene~~ temperatures in these regions. In CCSM in particular, the Eocene is characterised by a more globally equable precipitation rate: the expansion of zones of highest precipitation in the Eocene relative to preindustrial is muted compared with a more extensive loss of low precipitation regions. Additional support for this is provided by a comparison of mean precipitation rates for land and ocean (Table S2). The preindustrial ratio of land : ocean precipitation is maintained in the Eocene HadCM3L and ECHAM simulations, whereas in CCSM, precipitation rates over land and ocean are typically equal. The effects of differences in simulated surface air temperatures between models within the ensemble are also evident: for a given global surface temperature, HadCM3L maintains cooler poles than CCSM3 and ECHAM5 (Sect. 3.3.2) and regions with MAP< 300 cm year^{-1} persist in the Arctic and Antarctic, even at ×4 CO_2.

Modelled Eocene MAP features are frequently traceable to those identified in predindustrial simulations (Sect. 3.1), including the single tropical convergence zone in the GISS ×4 CO_2 simulation and the double ITCZ in a number of the models. Elsewhere, the Eocene precipitation distributions diverge from those of the preindustrial simulations and may be related to specific Eocene paleogeography, elevated CO_2, or other boundary conditions. In HadCM3L, there is a clear trend towards a more south-easterly trending SPCZ in the higher CO_2 simulations, which is not replicated in the warm simulations of the sister model FAMOUS. The SPCZ in CCSM is also far weaker in the Eocene simulations, compared to preindustrial simulations. The mechanisms which control the SPCZ in the modern day, particularly its northwest-southeast orientation, are only partially understood with zonal SST gradients, intensity of trade winds and the height of the Andes all suggested to be important influences (Matthews et al., 2012; Cai et al., 2012). In the EoMIP simulations, CCSM3 shows much slacker surface winds at the equator with reduced low-level convergence, whilst HadCM3L mantains stronger convergence of south-easterly trade winds with north-easterlies originating from the Pacific subtropical high (Fig S4). Despite similar preindustrial precipitation distributions over tropical Africa, CCSM and HadCM3L strongly diverge in the Eocene, with CCSM showing far more intense equatorial precipitation. In CCSM, evaporation is consistently less than the precipitation rate, which likely results in recharge of soil moisture throughout the year and an availability of moisture for convective precipitation.~~-~~The FAMOUS simulations E16 and E17 represent two realisations of very warm climates with a reduced equator-pole temperature gradient – in these simulations significant increases in mid-latitude precipitation are particularly accentuated over the Pacific Ocean; increases in convection in the subtropics and mid-latitudes are sufficient to eliminate the precipitation minima seen in other models at these latitudes.

For a given CO_2, differing boundary conditions, paramaterisation schemes and simulated model air temperatures prevent direct assessment of whether Eocene regional precipitation distributions are robust to GCM ~~selection~~choice. Model simulations have a substantially different amount of water vapour in the atmosphere and differing global precipitation rates and it is not meaningful to average these simulations. Instead, w~~W~~e show a multimodel mean in Fig. 5 for simulations with a common global precipitation rate to provide an assessment of regional variability between model simulations with the same global strength hydrological cycle~~.~~Elevated high-latitude precipitation for the early Eocene relative to preindustrial conditions is robust between GCMs, although absolute values remain variable between models, particularly in the Southern Hemisphere, likely due to differing Antarctic orography. Differences between models in the mid-latitudes are smaller, resulting in some confidence that the secondary precipitation maxima were polewards of their preindustrial location during the Eocene. Equatorial precipitation remains highly variable between models but is accentuated relative to preindustrial.

3.3.2 Controls on precipitation distribution

Precipitation rates for each simulation are summarised in Table S2, including separate rates calculated over land and ocean surfaces and rates deconvolved into those arising from convective and large-scale contributions. These data show that elevated precipitation rates in the high CO_2 Eocene simulations are largely the result of increased convection, although in the ECHAM5 model a greater percentage of precipitation is generated by large scale mechanisms in both the Eocene and preindustrial simulation. Figure 4 shows how convective and large-scale precipitation rates vary with latitude for a selection of the EoMIP simulations. This reveals differences between models in the mechanisms responsible for precipitation distributions which can be related to surface air temperature distributions. In the HadCM3L simulations, the mid-latitude maxima in both large scale and convective precipitation advance polewards with increasing CO_2 with precipitation increases over the high northern latitudes driven almost exclusively by enhanced large-scale precipitation. CCSM3 has substantially warmer poles which results in much enhanced high-latitude large scale precipitation relative to HadCM3L, although large scale latitudinal contributions differ somewhat for preindustrial simulations at both low and high latitudes. In CCSM3_K, the warmest CCSM3 simulations, polar temperatures are elevated compared to CCSM3_H as is total precipitation in these regions, but in this case large scale precipitation is reduced over much of the high latitudes and the higher total precipitation is due to convective processes. Mid-latitude precipitation maxima within the ECHAM5 simulation arise from large-scale mechanisms rather than convection; however, this is also true of the preindustrial simulation and does not relate to Eocene boundary conditions.

In the warmest FAMOUS simulations of Sagoo et al. (2013), the high latitudes experience particularly significant increases in large scale precipitation, such that the maximum values are those at the poles in the E17 simulation, and in the Southern Hemisphere the local mid-latitude precipitation maximum is lost. Elevated ~~mid-~~mid-latitude temperatures in the warm FAMOUS simulations additionally result in significant increases in convective precipitation which are not simulated in the cooler simulations and models. Overall, convective precipitation in FAMOUS increases as both global temperatures rise and equatorial-to-polar temperature gradients decrease, regardless of the underlying parameter configuration; this emphasises the fundamental control of temperature distribution on precipitation, as opposed to the effect of alteration of any one specific parameter.

Improvements in the simulation of precipitation in modern day climate simulations are often related to better resolved topography (e.g. Gent et al., 2010). However, given the variety of differences in boundary conditions between the EoMIP simulations, topography appears to only have limited power in explaining differences between regional precipitation responses. Figure S5 shows differences in topography and precipitation rate between three sets of simulations with similar global precipitation rates: (i) HadCM3L and FAMOUS – where the models have similar parameterisation schemes but differ in atmospheric grid resolution; (ii) CCSM3_W and HadCM3L – different models, but with a similar resolution; (iii) CCSM3_W and CCSM3_H – the same model but slightly different topographic boundary conditions. The HadCM3L and CCSM3_W simulations show some substantial differences in the topography around the Rockies, with the increased elevation in CCSM3 possibly accounting for the increased precipitation in this region. However, differences in topography over the Asian subcontinent do not result in any systematic differences in precipitation rate. Regions of similar topography elsewhere, including over the Tropics, have far more divergent precipitation responses between the models, which do not relate to local differences in topography.

For HadCM3L and CCSM3, simulations at different CO_2 concentrations provide an insight into how regional Eocene precipitation distributions are impacted by warming, and anomaly plots for high – low CO_2 simulations are shown in Fig. 6. For the same CO_2 forcing, CCSM3 is globally cooler than HadCM3L (Lunt et al., 2012), but the anomalies for 16 – 4 CO_2 (CCSM_W) and 6 – 2 CO_2 (HadCM3L) display similar global changes in both temperature and therefore precitation rate on account of similar d*P*/d*T* relationships (Fig. 2; Table 2). Intriguingly, HadCM3L displays far greater spatial contrasts in net precipitation change, particularly over the ocean: between the pair of HadCM3L simulations, some 23% of the Earth's surface experiences an increase or decrease in precipitation greater than 60 cm year^{-1}, compared to just 6% in the CCSM3 simulations. ~~Some spatial patterns are robust between models – including the dipole-like pattern over the Pacific, SPCZ migration, and subtropical reductions in precipitation at the expense of greater moisture transport to higher latitudes~~ Ignoring differences in the spatial pattern of atmospheric circulation - such as those relating to differing SPCZ (Sect 3.3.1), the underlying response appears to be an increase in precipitation in the deep tropics and a reduction in precipitation in the subtropics, at least over the Pacific Ocean. This increase in moisture in the convergence zone and decrease in the divergence zones appears to relate to a more vigorous change in tropical atmospheric circulation in the HadCM3L model relative to CCSM3 (Fig S~~5~~6) ~~.~~Other changes are model dependent: in HadCM3L, there is a clear increase in the strength of storm tracks along the eastern Asian coastline, which is not repeated in CCSM. In HadCM3L, ~~additional~~ decreases in precipitation occur around the Peri-Tethys and along the coastline of equatorial Africa. ~~Whilst~~ Therefore, although models within the EoMIP ensemble ~~therefore show~~exhibit similarities in their global rate of precipitation change with respect to temperature, regional precipitation distributions are strongly model dependent~~, diverging within the EoMIP ensemble according to surface air temperature characteristics.~~

3.4 Precipitation seasonality

The evolution and timing of the onset of global monsoon systems in the Eocene has been the subject of debate (Licht et al., 2014; Sun and Wang, 2005; Wang et al., 2013). Proxy studies for the early Eocene have highlighted differences in precipitation seasonality relative to modern (Greenwood et al., 2010; Greenwood, 1996; Schubert et al., 2012) and possible changes to seasonality at the PETM have also been invoked in a number of studies (Sluijs et al., 2011; Schmitz and Pujalte, 2007; Handley et al., 2012). Previous modelling work utilising CCSM3 has suggested that much of the mid-late Eocene was monsoonal, with up to 70% of annual rainfall occurring during one extended season in North and South Africa, North and South America, Australia and Indo-Asia (Huber and Goldner, 2012). Similarly, GCMs have been shown to differ greatly in their prediction of future monsoon systems (e.g. Turner and Slingo, 2009; Chen and Bordoni, 2014), therefore ~~so~~ we examine the similarities and differences in Eocene models with respect to the seasonality of their precipitation distributions.

Figure 7 shows the percentage of precipitation falling in the extended summer season (MJJAS for Northern Hemisphere; NDJFM for Southern Hemisphere) following the approach of Zhang and Wang (2008) and also utilised in the Eocene studies of Huber and Goldner (2012) and Licht et al. (2014). This metric has been shown to correlate well with the modern-day distribution of monsoon systems. Overall, the models show a global distribution of early Eocene monsoons in high CO_2 climates that is similar to those simulated under preindustrial simulations (Fig. ~~S6~~S7). Australia is markedly less monsoonal than in preindustrial simulations due to its more southerly Eocene paleolocation. Note that regions where winter season precipitation dominates fall at the lower end of the scale; these tend to be over the ocean surface but also include regions around the Peri-Tethys and both the Pacific and Atlantic US coasts.

HadCM3L is notable in that it is more seasonal at high latitudes, simulating an early Eocene monsoon centred over modern day Wilkes' Land region of Antarctica. Although proxy data have suggested highly seasonal precipitation regimes for both the Arctic (Schubert et al., 2012) and Antarctic (Jacques et al., 2014) during this interval, these systems are maximised in the ×2 CO_2 simulation and weaken somewhat in the simulations with elevated CO_2. This arises due to the high temperature seasonality of Arctic/ Antarctic Eocene regions in HadCM3L relative to the other models (e.g., Gasson et al., 2013). In austral winter, Antarctic temperatures are sufficiently low to suppress precipitation, ~~although~~ whilst this constraint is lifted somewhat in the higher CO_2 simulations which produce more equable rainfall distribution. The effect of elevated global warmth on the extent of Eocene monsoons is additionally consistent across the models, with a decline in terrestrial areas with seasonal precipitation regimes at higher CO_2 simulations (Table 3). HadCM3L simulates a 6% reduction in the extent of terrestrial regions influenced by monsoonal regimes for HadCM3L ×1 CO_2 relative to the preindustrial simulation, which appears to be related to the warmer surface temperatures and absence of Antarctic ice sheet.

3.5 *P* −*E* distributions

The difference between precipitation and evaporation (*P* −*E*) is ~~important to consider in the characterisation of~~essential for understanding the wider impacts of an enhanced Eocene hydrological cycle. Over land, this parameter broadly determines ~~the~~ how much of precipitation will ~~precipitation available to~~ become soil water and surface runoff, the partitioning itself being dependent on the land surface and vegetation schemes within the models (e.g. Cox et al., 1998; Oleson et al., 2004). Over the ocean, *P* −*E* drives differences in salinity which can affect the Eocene ocean circulation (Bice and Marotzke, 2001; Waddell and Moore, 2008). We show mean annual (*P* −*E*) budgets for each of the EoMIP simulations in Fig. 8. In warmer climates, an exacerbation of existing (*P* −*E*) is expected – that is, the wet become wetter and the dry drier, as the moisture fluxes associated with existing atmospheric circulations intensify (Held and Soden, 2006). Broadly, the EoMIP simulations support this paradigm for the Eocene relative to preindustrial (Fig. 5). CCSM3 shows fairly minor changes in the boundaries between net-precipitation and net-evaporation zones at higher CO_2 (Fig. 8), although the net-evaporation zones in HadCM3L do migrate polewards over the eastern Pacific and North Atlantic at high CO_2. Other dynamic changes within HadCM3L are coupled to the precipitation responses: the more meridionally-orientated SPCZ results in a weaker zonally averaged Southern Hemisphere evaporative zone ~~(Fig. 9)~~ and the expansion of precipitation along the Asian coastline results in a more positive ($P - E$) balance in this region. Over continents the models also display different responses of P-E to warming. For example, ~~Over~~ over equatorial and northern Africa, HadCM3L simulates increasingly wet climates in the high CO_2 simlations, driven by increases in precipitation coupled to reductions in evaporation. In CCSM3, the net moisture balance is less responsive with respect to temperature, although in~~s~~tense equatorial precipitation means this region is much wetter than in HadCM3L.

Because of the large latent heat fluxes involved in evaporation and condensation, the global hydrological cycle acts as a meridional transport of energy. Net evaporation in the subtropics stores energy in the atmosphere as latent heat, releasing it at high latitudes via precipitation (Pierrehumbert, 2002). An intensified hydrological cycle, associated with increased atmospheric transport of water vapour, has therefore been suggested as a potential mechanism for reducing the equator-pole temperature gradient during greenhouse climates (Ulfnar et al., 2004; Caballero and Langen, 2005). By integrating the area-weighted estimates of $P - E$ with latitude, we show how these contributions differ between the EoMIP models and associated preindustrial simulations in Fig. 9. Relative to preindustrial climatology, the intensification of the hydrological cycle associated with increased drying in the net-evaporative zones and increased moistening of the net-precipitation zones implies a stronger latent heat flux~~ and~~. ~~within~~ Within the EoMIP ensemble, the implied high polewards energy fluxes of the E16 and E17 FAMOUS simulations and ×2 CO_2 ECHAM simulation are particularly significant. GISS-ER has a particularly strong ~~low~~ low-latitude equatorially-directed latent heat transfer which arises from the much elevated Eocene precipitation rate in the deep tropics. The asymmetry in some of the models' implied flux is due to a hemispheric imbalance in precipitation/evaporation. For example, in FAMOUS e17 simulation, there is greater precipitation than evaporation in the southern hemisphere and so more energy is released from the atmosphere by latent heat than is stored, meaning that the implied heat flux does not cross zero at the equator. However, since total precipitation is equal to total evaporation globally (Table S1), this is balanced out in the northern hemisphere; note the intense evaporation zone over the North Atlantic is not matched in the Southern Hemisphere for this model. In the majority of the other models, there is greater symmetry in P-E with latitude and the implied flux crosses close to the origin of the graph on Figure 9.

At face value, it may seem that the elevated latent heat transport at mid to high latitudes could contribute towards the reduced equator-pole temperature gradient in the EoMIP simulations, but we note that theoretical and modelling based studies suggest increased latent heat transport is associated with an increased equator-pole temperature gradient (Pagani et al., 2014). Within the EoMIP ensemble, meridional temperature gradients and global surface air temperatures covary and so it is not possible to separate clearly the effects of these different controls (Fig. ~~S3~~S8). Nevertheless, these results illustrate that relative to preindustrial, the Eocene hydrological cycle acts ~~as~~ to elevate the meridional transport of latent heat, particularly around 45–50° N/S of the equator.

4 Proxy-model comparison

A range of proxy data provide constraints on how the early Eocene hydrological cycle differed to that of the modern, including oxygen isotopes from mammalian, fish and foraminiferal fossils (Clementz and Sewall, 2011; Zachos et al., 2006; Zacke et al., 2009) and the distribution of climatically sensitive sediments (e.g. Huber and Goldner, 2012). Changes in regional hydrology at the PETM have also been inferred from geomorphological (John et al., 2008; Schmitz and Pujalte, 2007), biomarker (Handley et al., 2011; Pagani et al., 2006) and microfossil (Sluijs et al., 2011; Kender et al., 2012) proxies. These have ~~often~~ resulted in qualitative interpretations of hydrological change, although the climatic variables and temporal signal the~~y~~ proxies record are often uncertain ~~in many instances~~ (e.g. Handley et al., 2011, 2012; Tipple et al., 2013; Sluijs et al., 2007). However, quantitative estimates of m~~M~~ean a~~A~~nnual p~~P~~recipitation (MAP), derived from micro- and macro-floral fossils have been made for a number of early Eocene and PETM-aged sections which can be compared directly with the GCM-estimated precipitation rates described in Sect. 3.

Paleoprecipitation estimates are primarily produced by two distinct paleobotanic methods – leaf physiogonomy and ~~Nearest~~ nearest ~~Living~~ living ~~Relative~~ relative (NLR) approaches. In the former, empirical univariate and multivariate relationships have been established between the size and shape of modern angiosperm leaves and the climate in which they grow, with smaller leaves predominating in low precipitation climates (e.g. Wolfe, 1993; Wilf et al., 1998; Royer et al., 2005). The NLR approach estimates paleoclimate by assuming fossilised specimens have the same climatic tolerances as their presumed extant relatives. This approach can utilise pollen, seeds and fruit in addition to leaf fossils (Mosbrugger et al., 2005). Relative to m~~M~~ean a~~A~~nnual air t~~T~~emperature, geologic estimates of

MAP are less precise, which may relate to decoupling between MAP and local water availability (Peppe et al., 2011; Royer et al., 2002), a greater importance of growing season climate (Mosbrugger and Utescher, 1997) or in the case of physiogonomical approaches, competing influence of other climatic variables on leaf form(Royer et al., 2007).

Our data compilation is provided in Table S3. Some of the data has been compared previously with precipitation rates from an atmosphere-only simulation performed with isoCAM3 for the Azolla interval (~ 49 Ma; Speelman et al., 2010). Our proxy-model comparison includes data for the remainder of the early-mid Eocene, including a number of recently-published estimates such that the geographic spread is widened to include estimates from Antarctica (Pross et al., 2012), Australia (Contreras et al., 2013; Greenwood et al., 2003), New Zealand (Pancost et al., 2013), South America (Wilf et al., 2005) and Europe (Eldrett et al., 2014; Mosbrugger et al., 2005; Geisental et al., 2011). We select Ypresian-aged data where multiple Eocene precip~~p~~itation rates exist, including estimates for the PETM (Pancost et al., 2013), but ~~have~~ additionally include~~d~~ some Lutetian and Paleocene data, particularly in regions where Ypresian data does not exist. This approach is justified in some respects given the range of plausible Eocene CO_2 with which simulations have been performed. However, each data point is an independent estimate of precipitation for a given point in time and direct comparisons between data points are hindered given that considerable climatic change occurred throughout this interval (e.g. Zachos et al., 2008).

Figure 10 shows paleobotanical estimates for MAP for a range of the data in Table S3~~2~~, along with model-estimated rates for each of the EoMIP simulations. Mean precipitation estimates from each model are derived by averaging over grid boxes centred on the paleolocation in a similar approach to Speelman et al. (2010). This is a nine cell grid of 3×3 gridboxes for HadCM3L, GISS, ECHAM and CCSM3, although in some instances an eight cell grid of 2×4 is used along paleocoastlines. Differing model resolutions and land–sea masks result in averaging signals from slightly different paleogeographic areas, but this approach allows for an assessment of the regional signal and error bars are included to show the range of precipitation rates present within the locally defined grid. In the reduced resolution model, FAMOUS, mean and range are derived from 2×2 gridboxes to ensure regional climatologies remains comparable. Error bars on the geologic data are generally provided as described in the original publications, with further details also provided in Table S3.

Our results confirm different regional sensitivities across the models. Over New Zealand (Fig. 10b), HadCM3L shows a strong sensitivity to increases in CO_2, whereas in CCSM3, elevated CO_2 has little effect on precipitation rate. This ~~can be interpreted in terms of the~~arises from differing SPCZ precipitation structures, with HadCM3L simulating a shift of the rain-belt towards New Zealand in the warmer simulations (Fig. 6). Conversely, in the Western US (Fig. 10g), HadCM3L precipitation is stable with respect to increases in CO_2 whilst CCSM3 produces increases in precipitation in higher CO_2 simulations. Furthermore, significant variations occur between the degree of match the models show with proxy precipitation estimates. At grid boxes corresponding to modern day Axel Heiberg Island (Fig. 10h), HadCM3L and GISS-ER are unable to produce sufficient precipitation, whereas the high CO_2 CCSM3 and E16/17 FAMOUS simulations are in closer agreement. Over Wilkes Land, Antarctica, all of the EoMIP models show sensitivity to CO_2, but ~~unanimously~~ all produce too little precipitation, although the FAMOUS and CCSM_K simulations with warmer polar temperatures (Fig. 4) come closest to replicating the central estimates of geologic data. However, some ~~(although some~~ caution is required in how these differencess are interpreted, given that preindustrial GCM errors are also typically of the order of 300 mm year^{-1} too little precipitation over this region~~)~~. A similar pattern is apparent in the Paleocene North West Territory data (Fig. 10l), with the models using low CO_2 and/or yielding cooler polar temperatures ~~cooler pole models and those at low CO_2~~ showing a dry bias. At the ~~mid-~~ mid-latitudes, model biases relative to paleoprecipitation estimates are reduced, including for the continental US (Fig. 10f), Argentina (Fig. 10g) and central Europe (Fig. 10m), where proxy data are within the precipitation range simulated across the suite of simulations.

At Tanzania (Fig. 10e), all model simulations appear to ~~overprecipitate~~ overestimate precipitation and in a number of models elevating CO_2 has relatively little impact on precipitation rate in a number of the models. In the HadCM3L simulations in particular, elevating CO_2 to levels required to produce a match with early Eocene high-latitude data results in considerable over-precipitation at this site~~.~~, although it should be noted that the Mahenge data are likely mid-Eocene in age, and could be representative of a lower CO_2 climate. With a scarcity of ~~low-~~ low-latitude data, this interpretation remains tentative, particularly given that a number of the models show a marginal preindustrial wet bias over tropical Africa (Fig. 1) and leaf physiognomic methods tend to result in lower precipitation estimates than those provided by other proxies (e.g., Peppe et al., 2011).

The ~~more~~ most robust observation from our comparison is that the models produce too little precipitation at locations corresponding to Eocene ~~high~~ high-latitude sites~~, and this~~ This is consistent with suggestions that GCMs fail to simulate high-latitude warmth for the Early Eocene~~.~~ given that If ~~high~~ high-latitude temperatures are too cold in the model, then the saturation vapour pressure of the atmosphere is suppressed ~~and polewards-moving airmasses lose moisture via rainout earlier in their trajectory~~. We demonstrate this coupling of data-model temperature and precipitation errors in Fig. ~~9~~11. In HadCM3L, increasing CO_2 from ×2 to ×6 decreases temperature and precipitation ~~anomalies~~ proxy-model differences at the majority of sites, resulting in better overall match to the geologic data. In the case of CCSM3, a relatively good match with precipitation proxy estimates is achieved at both low and high CO_2, but models appear too cold at low CO_2. In FAMOUS and CCSM3_K, parameter sets which reduce the equator-pole temperature gradient and warm the high latitudes are able to minimise errors in both temperature and precipitation with the majority of the geologic data at low CO_2. However, in FAMOUS, E17 simulates surface air temperatures> 45 °C in Colombia, which produces a significant temperature data-model anomaly.

Whilst our compilation allows for some degree of model intercomparison, it is far from a global data set, with a bias towards mid and high latitude sites, and a lack of data from low latitudes (~~Fig. S5~~Fig. 12; Fig S9~~; Fig S5~~). There is also a need for further proxy-model comparisons ~~from high latitudes~~ to corroborate our analysis. The paleobotanic estimates included here support the concept of a " fossil climate" at high latitudes – i.e. a paleoclimatic state with no modern analogue, which compromises the application of the ~~Nearest Living Relative~~NLR concept and leaf area analysis, especially given leaf size is thought to be a trade off between maximising photosynthesis and minimising water loss (Peppe et al., 2011). ~~Furthermore, on a warm Earth, the potential for decoupling between precipitation rate and water availability may have been enhanced at the high latitudes, particularly if increased precipitation was offset by elevated evaporation. Since $P - E$ is typically > 0 over land surfaces (Greve et al., 2014), land aridity indices such as P/PET which describe the atmopsheric water demand relative to the land surface may also assist in understanding demands on plants in a high CO_2 world.~~ The effect of a different Eocene seasonal cycle also requires further consideration. The models which are cooler at the poles such as HadCM3L show a stronger seasonal cycle in precipitation (Fig. 5) and analysis of growing season precipitation from these simulations may minimise the data-model anomaly we have described. Nonetheless, current best estimates of early and mid Eocene precipitation rate provide independent evidence for a proxy-model anomaly at high latitudes.

5 Conclusions

The simulations within the EoMIP ensemble support an intensified hydrological cycle for the early Eocene, characterised by enhanced global mean precipitation and evaporation rates and increased meridional latent heat transport. The sensitivity of Eocene precipitation rates to warming is within the range suggested for future IPCC-style climate change scenarios, although some variation is introduced by models which incorporate additional feedbacks such as the TRIFFID simulations of Loptson et al. (2014). Differences in Eocene surface temperature distributions drive differences between models in their regional precipitation rates including for models with similar global precipitation sensitivities (dP/dT). Anomalies between simulations at high and low CO_2 may provide a way by which to constrain changes in precipitation occurring during hyperthermals (Winguth et al., 2010). Regions which are particularly different between HadCM3L and CCSM3 include coastal regions around the Peri-Tethys, the South Pacific, and tropical Africa which may represent targets for future proxy-data acquisition. We additionally show a summary of where the greatest model spread in some of the simulations of the EoMIP ensemble can be found, along with the existing paleobotanic precipitation estimates in Figure 12. This emphasises the need for additional data from the low latitudes in order to assess which models perform most realistically. ~~The modern-day distribution of monsoons appears largely similar to that of the early Eocene across the EoMIP ensemble and the presence of monsoons across a range of CO_2 corroborates the work of Huber and Goldner (2012). The results suggest a decline in the extent of monsoon-influenced terrestrial regions in high-CO_2, warm climates, which may have implications for the interpretation of proxy data from hyperthermal events, such as the PETM, and for understanding the long-term evolution of monsoon systems.~~ There is now a need to move towards coordinated Eocene experiments between modelling groups which will improve the ability to mechanistically explain inter-model differences. Simulations with higher resolution 'state-of-the-art' GCMs would also be valuable, given the impacts that improved representation of orography and smaller scale atmospheric dynamics have had in reducing biases such as double ITCZ, representation of storm tracks and monsoon precipitation (~~e.g.~~ Hack et al., 2006; Delworth et al., 2012; Gent et al., 2010).

Our proxy comparison emphasises the coupling between temperature and precipitation data-model anomalies. For ~~high-~~high-latitude sites, model simulations are typically too cold, resulting in suppressed precipitation across a number of the models. Model simulations which enhance high-latitude warmth are in better agreement with existing proxy data, but the size of precipitation error bars prevents an identification of a “best” simulation. Models which warm the poles via high CO_2 (Liu et al., 2009; Winguth et al., 2010) are equally successful as models which achieve warmth at low CO_2 ~~via~~ by varying poorly constrained parameter values (Sagoo et al., 2013; Kiehl and Shields, 2013). Better constraints on uncertain early Eocene boundary conditions, including CO_2, and more data from low latitudes are now required, as are other proxy approaches which can verify the ~~high-~~high-latitude anomaly we have observed. Forward proxy modelling of water isotopes (Speelman et al., 2010; Sturm et al., 2009; Tindall et al., 2010) and comparison to archives which incorporate an Eocene δD or $\delta^{18}O$ signal (Zacke et al., 2009; Krishnan et al., 2014; Fricke and Wing, 2004) represents one such avenue.

Proxies sensitive to hydrological changes offer an independent means to temperature by which to assess paleoclimatic model performance. Whilst elevated CO_2 causes a near-global increase in model-simulated surface temperatures, the same warming results in regions of both increased and reduced precipitation and $P-E$ within climate models ~~.~~(Figs. 5 and 9) Even without tightly constrained absolute changes in precipitation or net hydrological balance, the spatial pattern of qualitative indicators may ~~therefore provide~~prove a critical test of GCM ability for warm paleoclimates. Where estimates of absolute precipitation rates do exist, our preliminary model-data comparison indicates that GCMs are broadly unable to simulate sufficient high-latitude precipitation for the early Eocene, even with CO_2 configured at the upper end of proxy inferred estimates. Precipitation biases within models are coupled to those of temperature and our analysis is therefore consistent with the prevailing view of enhanced early Eocene ~~high~~ high-latitude warmth. Our study represents a first step towards characterising the variability of the Eocene hydrological cycle simulated in GCMs. Further work is now required to study how other modelled aspects of the hydrological cycle such as runoff and salinity vary within the Eocene, and how these hydrological changes may relate to signals preserved in the geological record.

The Supplement related to this article is available online at doi:10.5194/cpd-11-3277-2015-supplement.

Acknowledgements

DJL acknowledges support through the NERC grant Cretaceous-Paleocene-Eocene: Exploring Climate and Climate Sensitivity (NE/K014757/1). RDP acknowledges the Royal Society for a Wolfson Research Merit Award. Finally, we thank two anonymous reviewers for their constructive comments which improved the quality of this manuscript.

Following references need to be added to the manuscript

Bony, S., Bellon, G., Klocke, D., Sherwood, S., Fermepin, S., & Denvil, S. (2013). Robust direct effect of carbon dioxide on tropical circulation and regional precipitation. *Nature Geoscience*, *6*, 447–451. doi:10.1038/ngeo1799

Brown, J. R., Power, S. B., Delage, F. P., Colman, R. a., Moise, A. F., & Murphy, B. F. (2011). Evaluation of the South Pacific convergence zone in IPCC AR4 climate model simulations of the twentieth century. *Journal of Climate*, *24*, 1565–1582. doi:10.1175/2010JCLI3942.1

Brown, J. R., Power, S. B., Delage, F. P., Colman, R. a., Moise, A. F., & Murphy, B. F. (2011). Evaluation of the South Pacific convergence zone in IPCC AR4 climate model simulations of the twentieth century. *Journal of Climate*, *24*, 1565–1582. doi:10.1175/2010JCLI3942.1

Cai, W., Lengaigne, M., Borlace, S., Collins, M., Cowan, T., McPhaden, M. J., Timmermann, A., Power, S., Brown, J., Menkes, C., Ngari, A., Vincent, E.M., Widlansky, M. J. (2012). More extreme swings of the South Pacific convergence zone due to greenhouse warming. *Nature*, *488*, 365–369. doi:10.1038/nature11358

Chadwick, R., Boutle, I., & Martin, G. (2012). Spatial Patterns of Precipitation Change in CMIP5: Why the Rich Do Not Get Richer in the Tropics. *Journal of Climate*, *26*, 3803–3822. doi:10.1175/JCLI-D-12-00543.1

Chou, C., & Neelin, J. D. (2004). Mechanisms of Global Warming Impacts on Regional Tropical Precipitation*. *Journal of Climate*, *17*(13), 2688–2701. doi:10.1175/1520-0442(2004)017<2688:MOGWIO>2.0.CO;2

Chou, C., Neelin, J. D., Chen, C. A., & Tu, J. Y. (2009). Evaluating the “rich-get-richer” mechanism in tropical precipitation change under global warming. *Journal of Climate*, *22*, 1982–2005. doi:10.1175/2008JCLI2471.1

Dee, D. P., Uppala, S. M., Simmons, a. J., Berrisford, P., Poli, P., Kobayashi, S., Andrae, U., Balmaseda, M.A., Balsamo, G., Bauer, P., Bechtold, P., Beljaars, A.C.M., Van de Berg, L., Bidlot, J., Bormann, N., Delsol, C., Dragani, R., Fuentes, M., Geer, A.J., Haimberger, L., Healy, S.B., Hersbach, H., Hólm, E.V., Isaksen, L., Kållberg, P., Köhler, M., Matricardi, M., Mcnally, A.P., Monge-Sanz, B.M., Morcrette, J.J., Park, B.K., Peubey, C., de Rosnay, P., Tavolato, C., Thépaut, J.N., Vitart, F. (2011). The ERA-Interim reanalysis: Configuration and performance of the data assimilation system. *Quarterly Journal of the Royal Meteorological Society*, *137*, 553–597. doi:10.1002/qj.828

Delworth, T. L., Rosati, A., Anderson, W., Adcroft, A. J., Balaji, V., Benson, R., … Zhang, R. (2012). Simulated climate and climate change in the GFDL CM2.5 high-resolution coupled climate model. *Journal of Climate*, *25*, 2755–2781. doi:10.1175/JCLI-D-11-00316.1

Gasson, E., Lunt, D. J., DeConto, R., Goldner, A., Heinemann, M., Huber, M., LeGrande, A.N., Pollard, D., Sagoo, N., Siddall, M., Winguth, A., Valdes, P. J. (2014). Uncertainties in the modelled CO2 threshold for Antarctic glaciation. *Climate of the Past*, *10*(2), 451–466. doi:DOI 10.5194/cp-10-451-2014

Gent, P., Yeager, S., Neale, R., Levis, S., & Bailey, D. (2010). Improvements in a half degree atmosphere/land version of the CCSM. *Climate Dynamics*, *34*(6), 819–833. doi:10.1007/s00382-009-0614-8

Held, I. M., & Soden, B. J. (2006). Robust responses of the hydrological cycle to global warming. *Journal of Climate*, *19*, 5686–5699. doi:10.1175/JCLI3990.1

Huber, M., Brinkhuis, H., Stickley, C. E., Döös, K., Sluijs, A., Warnaar, J., Schellenberg, S.A., Williams, G. L. (2004). Eocene circulation of the Southern Ocean: Was Antarctica kept warm by subtropical waters? *Paleoceanography*, *19*, 1–12. doi:10.1029/2004PA001014

Inglis, G.N., Farnsworth, A., Lunt, D., Foster, G.L., Hollis, C.J., Pagani, M., Jardine, P., Pearson, P.N., Markwick, P., Galsworthy, A., Raynham, A., Taylor, K.W.R. and Pancost, R.D. (2015), Descent towards the Icehouse: Eocene sea surface cooling inferred from GDGT distributions, *Paleoceanography*, 30, 1000 – 1020. doi: 10.1002/2014PA002723

Joetzjer, E., Douville, H., Delire, C., & Ciais, P. (2013). Present-day and future Amazonian precipitation in global climate models: CMIP5 versus CMIP3. *Climate Dynamics*, *41*, 2921–2936. doi:10.1007/s00382-012-1644-1

Kirk-Davidoff, D. B. (2002). On the feedback of stratospheric clouds on polar climate. *Geophysical Research Letters*, *29*, 1–4. doi:10.1029/2002GL014659

Korty, R. L., Emanuel, K. a., & Scott, J. R. (2008). Tropical cyclone-induced upper-ocean mixing and climate: Application to equable climates. *Journal of Climate*, *21*, 638–654. doi:10.1175/2007JCLI1659.1

Lin, J-L. L. (2007). The double-ITCZ problem in IPCC AR4 coupled GCMs: Ocean-atmosphere feedback analysis. *Journal of Climate*, *20*, 4497–4525. doi:10.1175/JCLI4272.1

Liu, C., Allan, R. P., Brooks, M., & Milton, S. (2014). Comparing tropical precipitation simulated by the Met Office NWP and climate models with satellite observations. *Journal of Applied Meteorology and Climatology*, *53*, 200–214. doi:10.1175/JAMC-D-13-082.1

Matthews, A. J. (2012). A multiscale framework for the origin and variability of the South Pacific Convergence Zone. *Quarterly Journal of the Royal Meteorological Society*, *138*(666), 1165–1178. doi:10.1002/qj.1870

Mehran, A., AghaKouchak, A., & Phillips, T. J. (2014). Evaluation of CMIP5 continental precipitation simulations relative to satellite-based gauge-adjusted observations. *Journal of Geophysical Research*, 1–17. doi:10.1002/2013JD021272.

Phillips, T. J., & Gleckler, P. J. (2006). Evaluation of continental precipitation in 20th century climate simulations: The utility of multimodel statistics. *Water Resources Research*, *42*, W03202. doi:10.1029/2005WR004313

Replace Hack et al. (2006) citation with:

Hack, J. J., Caron, J. M., Danabasoglu, G., Oleson, K. W., Bitz, C., & Truesdale, J. E. (2006). CCSM–CAM3 Climate Simulation Sensitivity to Changes in Horizontal Resolution. *Journal of Climate*, *19*, 2267–2289. doi:10.1175/JCLI3764.1

Figure changes for *Carmichael et al.*
A model-model and model-data comparison for the early Eocene hydrological cycle

Figure 1
No changes.

Figure 2
No changes.

Figure 3
No changes.

Figure 4
Replacement Figure 4.

Figure 4. Latitudinal temperature and precipitation distributions in the HadCM3L and ECHAM5 (left), CCSM3_H and CCSM3_K (centre) and FAMOUS (right) members of the EoMIP ensemble. **(a–c)** show mean surface air temperature, **(d–f)** total precipitation rate, **(g–i)** convective precipitation and **(j–l)** large-scale precipitation. The HadCM3L, ECHAM5 and CCSM3 atmospheric CO2 levels are shown in the key. All FAMOUS simulations are at 2_PI CO2, but differ in value for 10 uncertain parameters (Sect. 2). Simulation names E1–E17 shown in the legend correspond to those given by Sagoo et al. (2013). Black dotted lines show output from preindustrial simulations~~.~~, with the exception of ECHAM5, shown in orange.

Figure 5
No changes.

Figure 6
No changes.

Figure 7
No changes.

Figure 8
No changes.

Figure 9
Replacement Figure 9.

Figure 9. Latitudinal ~~*P – E*~~ *E - P* distributions (top) and implied northwards latent heat flux (bottom) in the EoMIP simulations. The black lines indicate preindustrial simulations with dotted and unbroken lines in (**d** and **h**) corresponding to the GISS-ER and ECHAM5 simulations respectively. Heat flux expressed in petawatts (1PW= 1015 W). Observational E – P in (a) is based on ECMWF ERA reanalysis data (Dee et al., 2004).

Figure 10
Replacement Figure 10.

No change required to caption.

Figure 11
No changes.

Figure 12
New Figure 12.

Figure 12 Summary of regions which show a significant model spread, based on the Eocene multimodel mean described in Figure 5. Paleobotanical estimates of quantitative precipitation rate included in the data compilation are shown by green markers. Regions where the standard deviation is greater than 1 mm/day are marked by a red outline and regions where the coefficient of variation (standard deviation/multimodel mean) is greater than 40% are outlined blue.

Table 1
Updated with Replacement Table 1. This includes changes to the caption.

Figure Captions

Figure 1 Preindustrial precipitation distributions as simulated in the EoMIP models. Panels a, b, d, f, h, j and l show Mean Annual Precipitation (MAP; left colour bar) and panels c, e, g, i, k, and m show anomalies relative to CMAP observations, 1979 – 2010, GCM output – observations (right colour bar).

Figure 2 Global sensitivity of the Eocene hydrological cycle in the EoMIP simulations. Global mean surface air temperature relative to model CO_2 (a), global mean precipitation rate relative to model CO2 (b) and global mean surface air temperature (c); note the logarithmic scale on the horizontal axis in (a) and (b). Preindustrial simulations and Eocene simulations are shown as circles and squares respectively. The CCSM3 simulations share a preindustrial simulation, shown in green. Open circle symbols in (b) show modern day estimates of global precipitation rate calculated based on CMAP data (red), GPCP data (blue) and Legates and Willmott (1990) climatology (green). Also shown is the sensitivity of the hydrological cycle to global mean Surface Air Temperature in the 17 successful simulations of Sagoo et al. (2013) using FAMOUS (d; blue squares), with HadCM3L simulations (red; Lunt et al., 2010) shown for comparison. All best fit lines are based on Eocene simulations only.

Figure 3 Mean annual precipitation distributions for each member of the EoMIP ensemble in cm/yr. CO_2 for each model simulation is shown above each plot. The FAMOUS simulations are both at 2 x $CO_{2.}$

Figure 5 Multimodel Mean Annual Precipitation (a) and Mean Annual Precipitation – Evaporation rate (b) for Eocene (red) and preindustrial (blue) boundary conditions. For the Eocene multimodel mean, simulations have a global mean precipitation rate of 3.40+/-0.02 mm/day which are: HadCM3L (x4), HadCM3L_T (x4), ECHAM (x2), CCSM3_H (x4) and a linearly interpolated distribution between the x4 and x8 CO2 CCSM3_W simulations. Error bars represent the range in values across simulations.

Figure 6 Anomaly plots for Mean Annual Precipitation cm/yr between high and low CO_2 model simulations for (a) HadCM3L x6 CO_2 – x2 CO_2 and (b) CCSM3_W x16 CO_2 – x4 $CO_{2.}$

Figure 7 Percentage of mean annual precipitation falling in the extended summer season (MJJAS for northern hemisphere, NDJFM for southern hemisphere); regions with >55% summer precipitation are outlined in blue. Results from preindustrial simulations are shown in the Appendix. CO_2 for each model simulation is shown above each plot. The FAMOUS simulations are both at 2 x $CO_{2.}$

Figure 8 Mean annual P-E distributions for each member of the EoMIP ensemble in mm/day. CO_2 for each model simulation is shown above each plot. The FAMOUS simulations are both at 2 x $CO_{2\,,.}$

Figure 10 Proxy-model comparisons for Mean Annual Precipitation (MAP) for the EoMIP ensemble a) Chickaloon Fm, Alaska; data from Sunderlin et al., 2011,2014; b) Waipara, New Zealand; data from Pancost et al., 2013; c) South East Australia and Tasmania; d) Wilkes Land; data from Pross et al., 2012; data from Greenwood et al., 2005 and Contreras et al., 2014; e) Tanzania; data from Jacobs and Herendeen, 2004 and Kaiser et al., 2006; f) Patagonia; data from Wilf et al., 2005.; g) Western US; data presented in Wing et al., 1993 and recalibrated by Wilf et al., 1998; h) i) Axel Heiberg island; data from Greenwood et al., 2010; j) ODP Site 913; data from Eldrett et al., 2009; k) Cerrejon Formation, Colombia; Wing et al. (2009); l) North West Territory; Greenwood et al., 2010; m) central Europe; Mosbrugger et al., 2005; Grein et al., 2011. Error bars show the mean with range based on nine model grid cells closest to given paleocoordinates. Full details are given in Supplementary Information Table S3.

Figure 11 Surface air temperature and mean annual precipitation proxy-model anomalies for low and high CO_2 climates shown by closed and open circles respectively. Simulations are at x2 and x6 CO_2 for HadCM3L (a), e17 for FAMOUS (b), x2 and x16 CO_2 for CCSM3_H (c), and x5 and x9 CO_2 for CCSM3_K (d). The data points represent averaged signals for the sites shown in Figure 8. Estimates of maximum(minimum) error are calculated as anomalies between the highest(lowest) data estimate and the lowest(highest) value within the local model grid.

Figure S1 Percentage error between preindustrial model simulated Mean Annual Precipitation and CMAP observational data, calculated as (model-observations)/observations x 100%

Figure S2 Coefficient of variation for preindustrial model simulations, calculated as standard deviation of multi-model mean (n=5) divided by multi-model mean. This is robust against larger standard deviations in regions of higher precipitation.

Figure S3 Changes in mean annual evapotranspiration 4 x CO_2 – 2 CO_2 simulations in HadCM3L in (a) the fixed shrubland simulations of Lunt et al. (2010) and (b) the TRIFFID dynamic vegetation simulations of Loptson et al. (2014). The differences in mean specific humidity relative to air temperature over tropical continents is shown in (c).

Figure S4 Surface pressure and winds over the South Pacific in Eocene simulations (a) HadCM3L, 2 x CO_2 and (b) CCSM3W, 4 x CO_2. The length of vectors is proportional to wind strength. The blue line shows the outline of the region where mean precipitation is greater than 5 mm/day.

Figure S5 Differences in topography (a – c) and precipitation rate (d – f) in pairs of simulations; HadCM3L 6 x CO2 – CCSM3H 8 x CO2 (a,d); HadCM3L 4 x CO2 – FAMOUS e10 (b,e) and CCSM3H 4 x CO2 and CCSM3W 8xCO2. Simulations are chosen which have similar global precipitation rates (Figure 2).

Figure S6 Vertical velocity of atmosphere averaged over 150°E to 150°W for HadCM3L simulations (left) and CCSM3(W) simulations (right). The bottom figures shows anomalies for the high CO_2 – low CO_2 simulations.

Figure S7 Percentage of mean annual precipitation falling in the extended summer season (MJJAS for northern hemisphere, NDJFM for southern hemisphere) for preindustrial simulations; regions with >55% summer precipitation are outlined in blue.

Figure S8 Variations in the peak extratropical (>25°N/S) latent heat flux in petawatts (1 PW = 10^{15} W) between the EoMIP model simulations relative to global mean surface air temperature and the average difference in surface air temperature between the poles and equator. With the exception of the FAMOUS simulations of Sagoo et al. (2013), we join simulations performed with the same GCM for clarity.

Figure S9 Proxy estimates of mean annual precipitation shown relative to latitudinal precipitation distribution for each of the EoMIP simulations. Model CO_2 or simulation name in the case of FAMOUS are shown above each panel. Preindustrial precipitation is shown as a black dotted line. Geologic data are represented by a lower, central and upper estimate based on combined data for the following sites: Wilkes Land, Antarctic Peninsula, southern Australia, New Zealand, Chile, Tanzania, Colombia, eastern China, continental US, central Europe, North West Territories, Alaska, Site 913 and Axel Heiberg Island. Model estimates from gridboxes corresponding to the paleo-locations are shown as coloured circles.

Figure 1

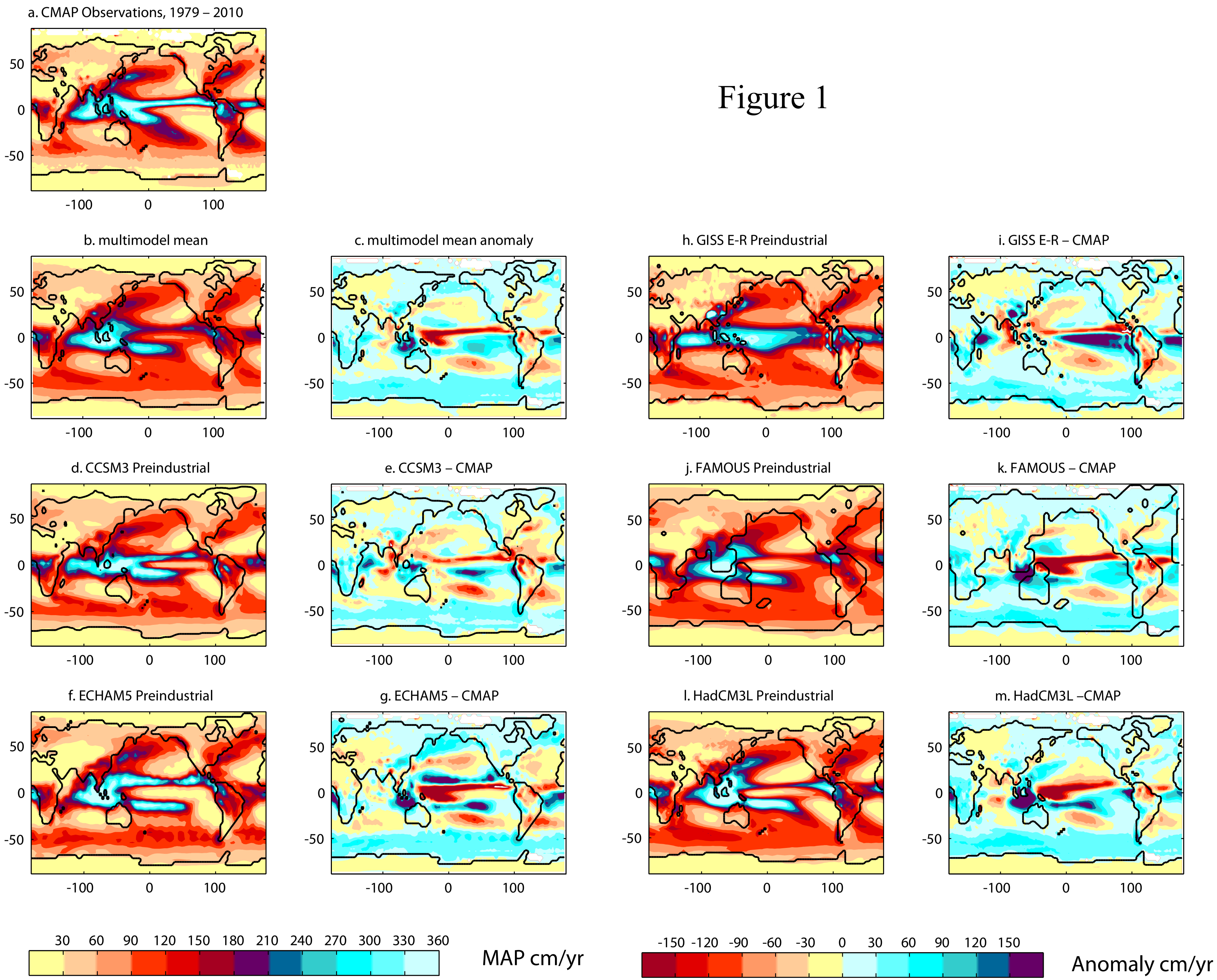
a. CMAP Observations, 1979 – 2010
b. multimodel mean
c. multimodel mean anomaly
d. CCSM3 Preindustrial
e. CCSM3 – CMAP
f. ECHAM5 Preindustrial
g. ECHAM5 – CMAP
h. GISS E-R Preindustrial
i. GISS E-R – CMAP
j. FAMOUS Preindustrial
k. FAMOUS – CMAP
l. HadCM3L Preindustrial
m. HadCM3L –CMAP
50
0
-50
-100
0
100
30 60 90 120 150 180 210 240 270 300 330 360
MAP cm/yr
-150 -120 -90 -60 -30 0 30 60 90 120 150
Anomaly cm/yr

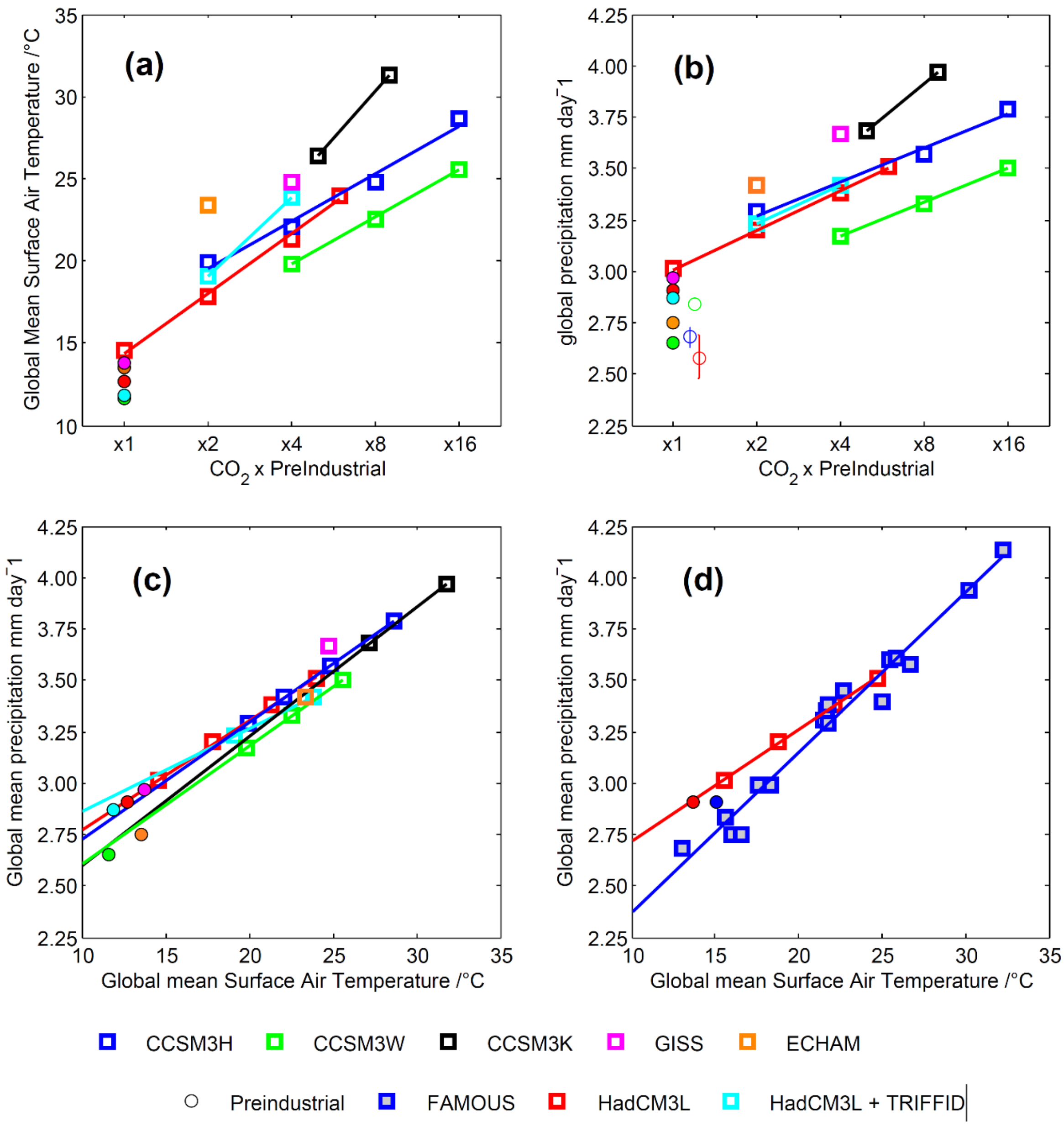

(a)
Global Mean Surface Air Temperature /°C
CO2 x PreIndustrial
x1
x2
x4
x8
x16
(b)
global precipitation mm day⁻1
CO2 x PreIndustrial
(c)
Global mean precipitation mm day⁻1
Global mean Surface Air Temperature /°C
(d)
Global mean precipitation mm day⁻1
Global mean Surface Air Temperature /°C
CCSM3H
CCSM3W
CCSM3K
GISS
ECHAM
Preindustrial
FAMOUS
HadCM3L
HadCM3L + TRIFFID

Figure 2

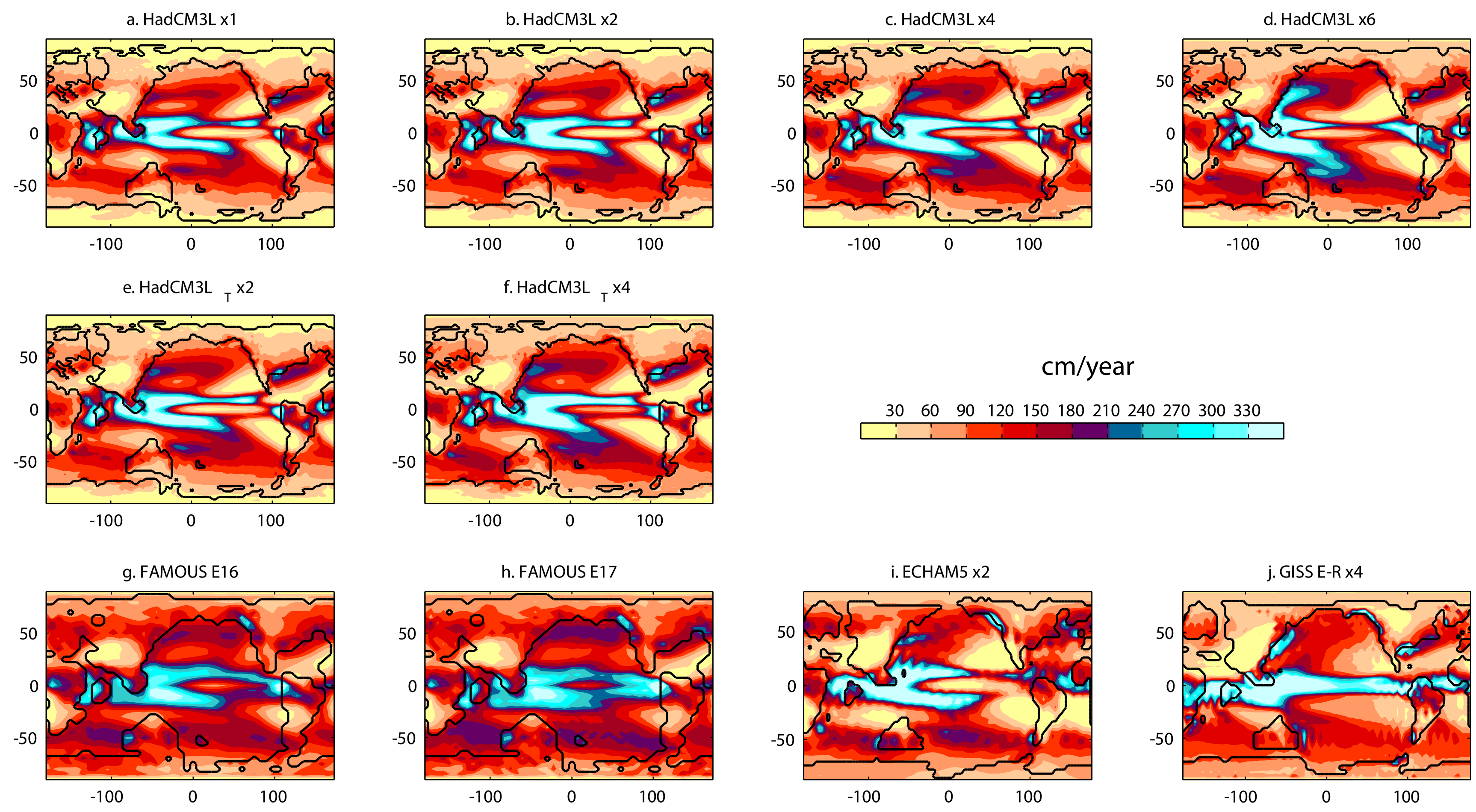
a. HadCM3L x1
b. HadCM3L x2
c. HadCM3L x4
d. HadCM3L x6
e. HadCM3L $_T$ x2
f. HadCM3L $_T$ x4
g. FAMOUS E16
h. FAMOUS E17
i. ECHAM5 x2
j. GISS E-R x4
cm/year
30 60 90 120 150 180 210 240 270 300 330
50
0
-50
-100
100

Figure 3a

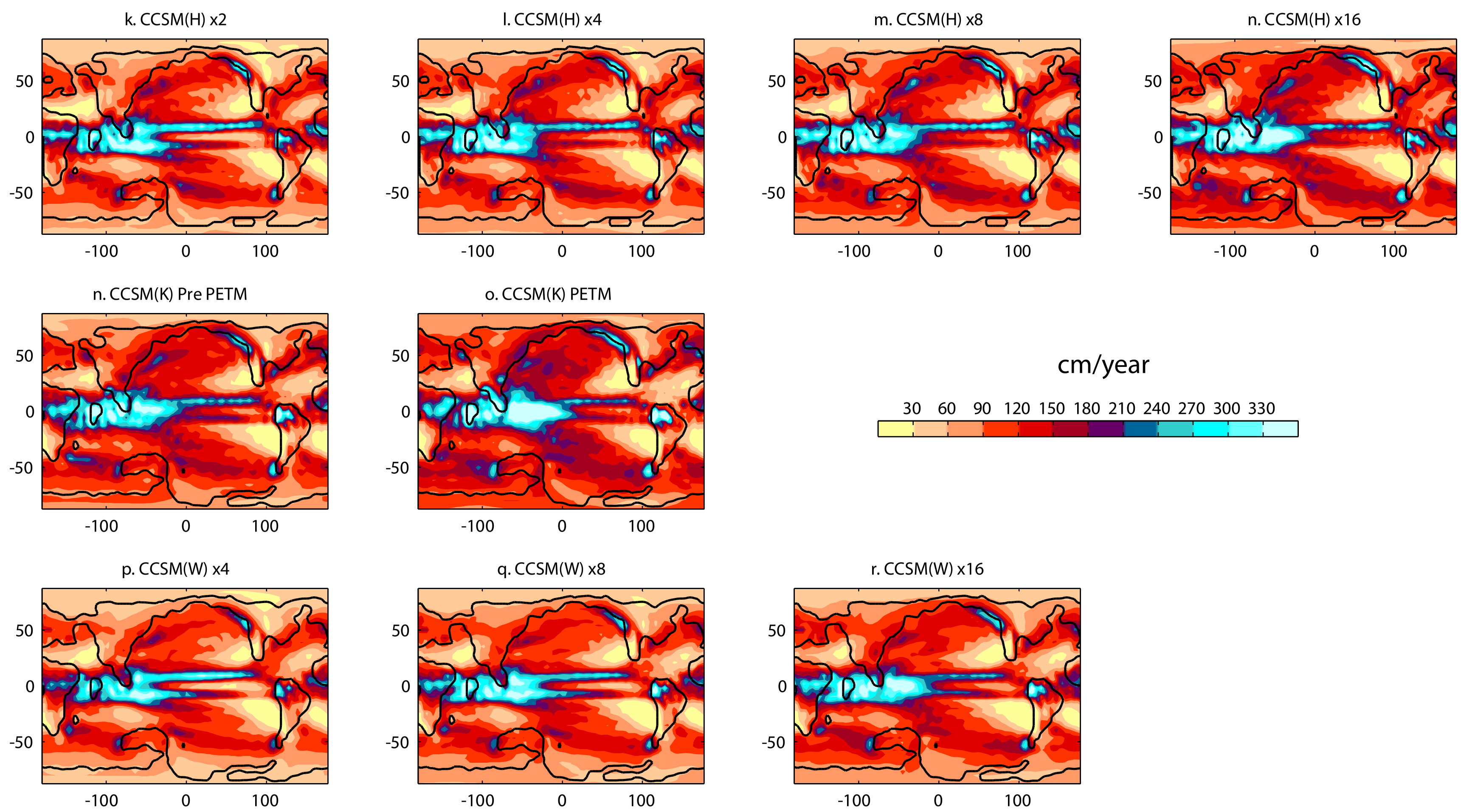
k. CCSM(H) x2
l. CCSM(H) x4
m. CCSM(H) x8
n. CCSM(H) x16
n. CCSM(K) Pre PETM
o. CCSM(K) PETM
p. CCSM(W) x4
q. CCSM(W) x8
r. CCSM(W) x16
cm/year
30 60 90 120 150 180 210 240 270 300 330
50
0
-50
-100
0
100

Figure 3b

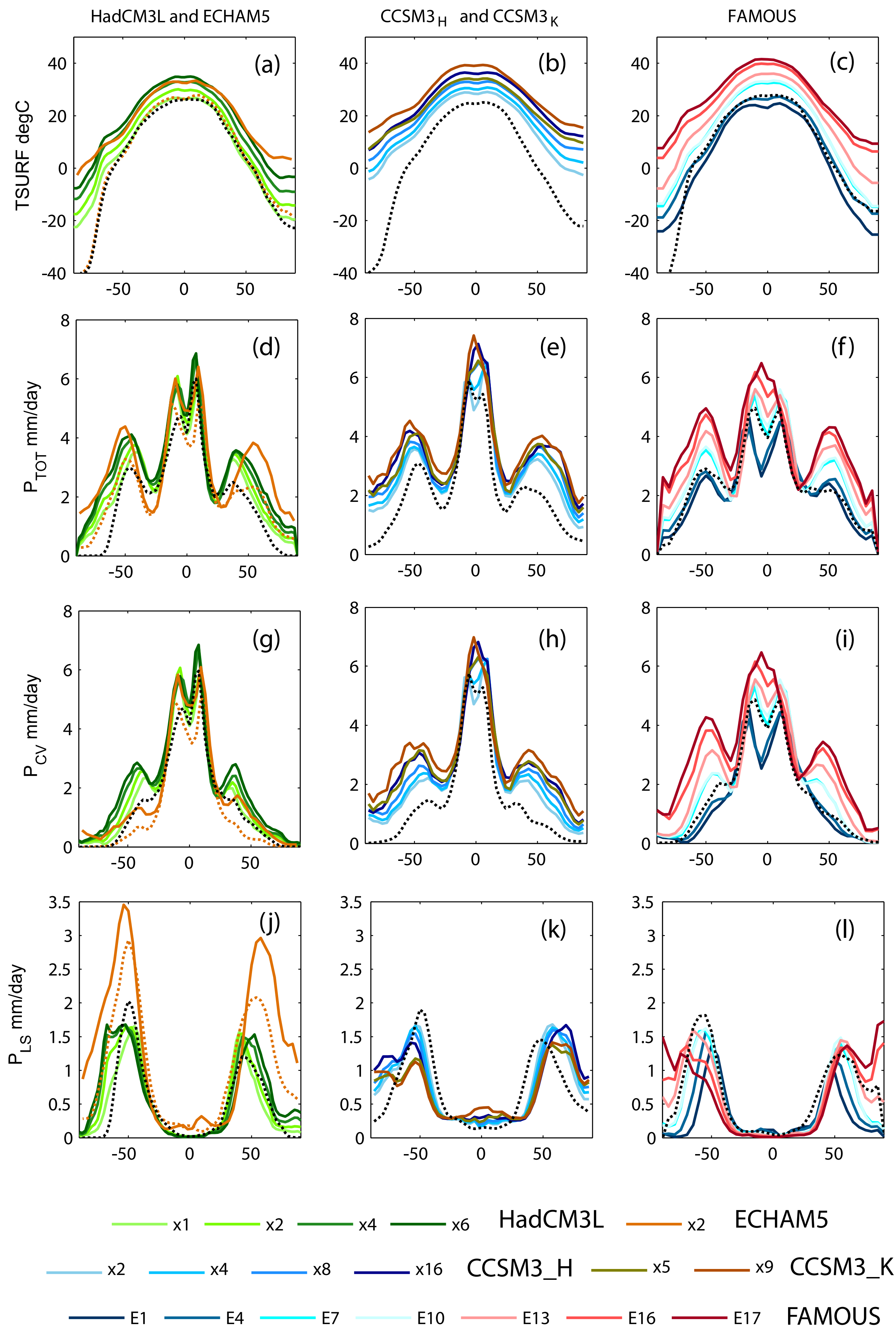

HadCM3L and ECHAM5
CCSM3 H and CCSM3 K
FAMOUS
TSURF degC
P_{TOT} mm/day
P_{CV} mm/day
P_{LS} mm/day
(a)
(b)
(c)
(d)
(e)
(f)
(g)
(h)
(i)
(j)
(k)
(l)
x1 x2 x4 x6 HadCM3L x2 ECHAM5
x2 x4 x8 x16 CCSM3_H x5 x9 CCSM3_K
E1 E4 E7 E10 E13 E16 E17 FAMOUS

Figure 4

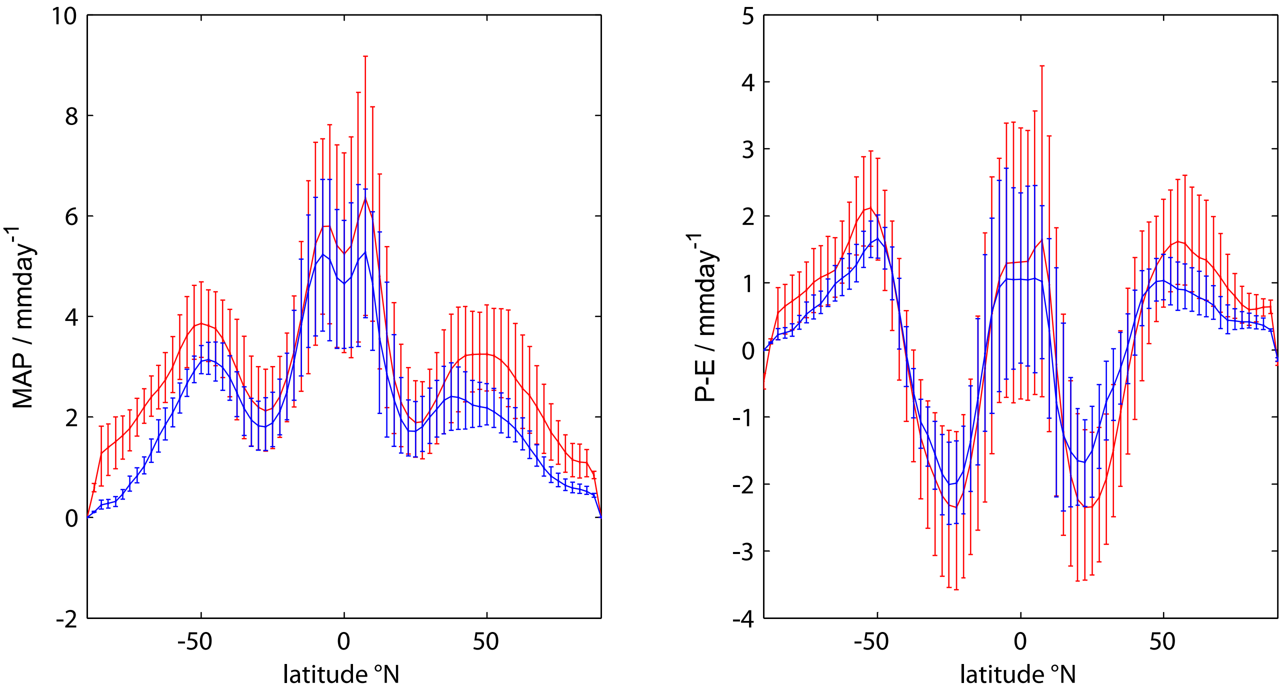
MAP / mmday-1
P-E / mmday-1
latitude °N
latitude °N
10
8
6
4
2
0
-2
5
4
3
2
1
0
-1
-2
-3
-4
-50
0
50
-50
0
50

Figure 5

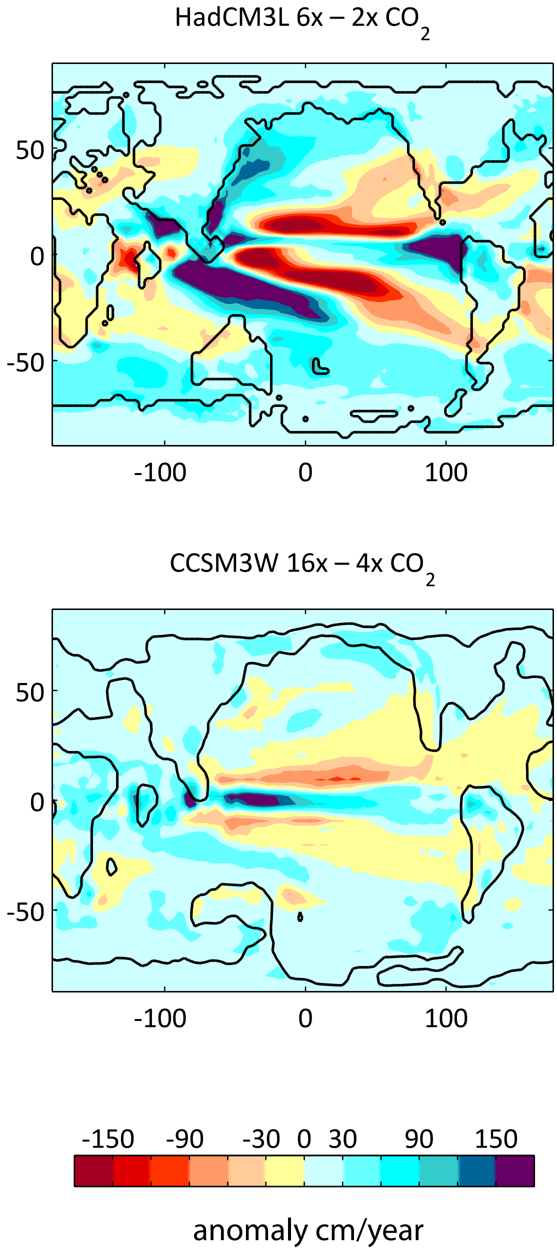
HadCM3L 6x – 2x CO2
50
0
-50
-100
0
100
CCSM3W 16x – 4x CO2
50
0
-50
-100
0
100
-150
-90
-30
0
30
90
150
anomaly cm/year

Figure 6

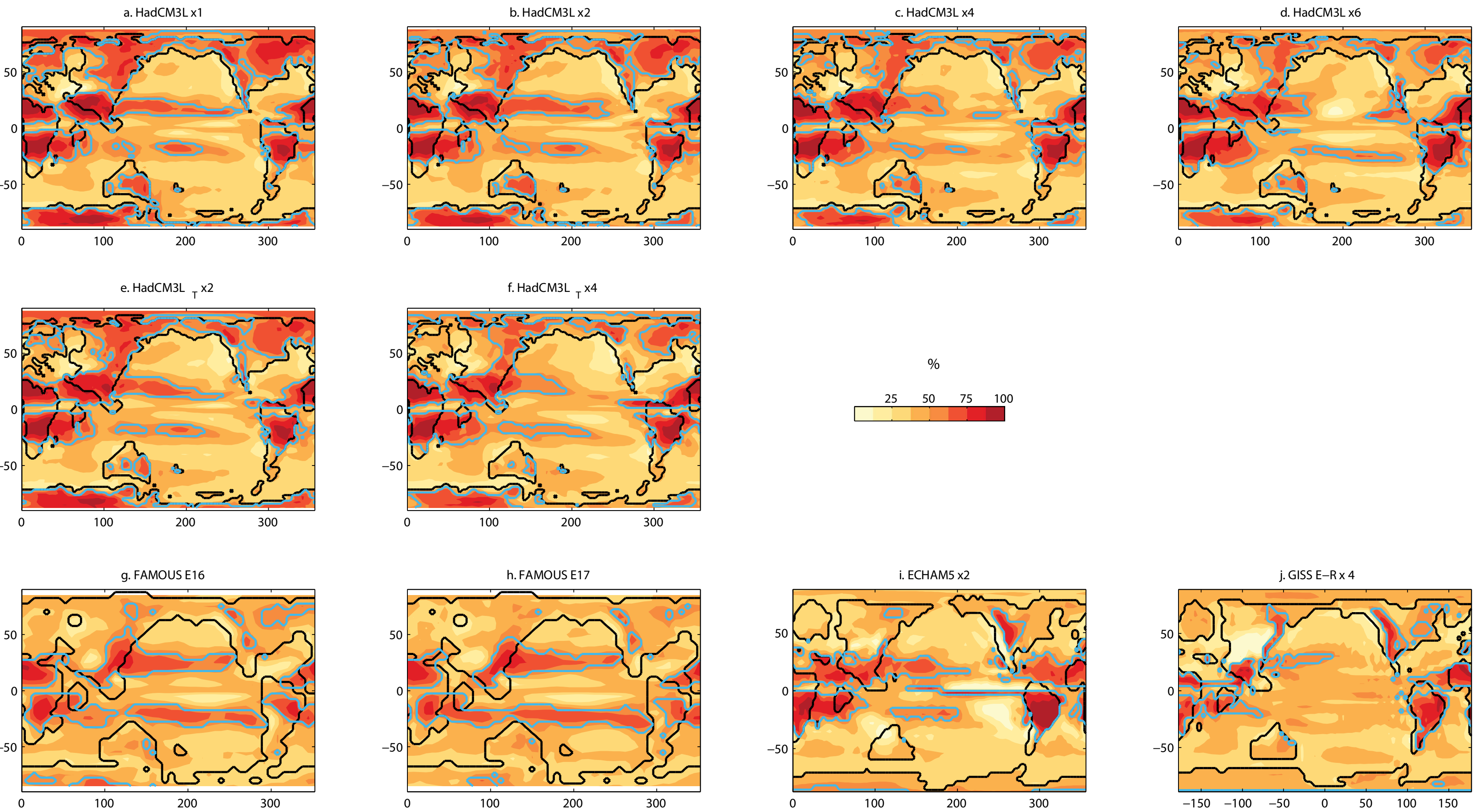
a. HadCM3L x1
b. HadCM3L x2
c. HadCM3L x4
d. HadCM3L x6
e. HadCM3L T x2
f. HadCM3L T x4
%
25
50
75
100
g. FAMOUS E16
h. FAMOUS E17
i. ECHAM5 x2
j. GISS E−R x 4

Figure 7a

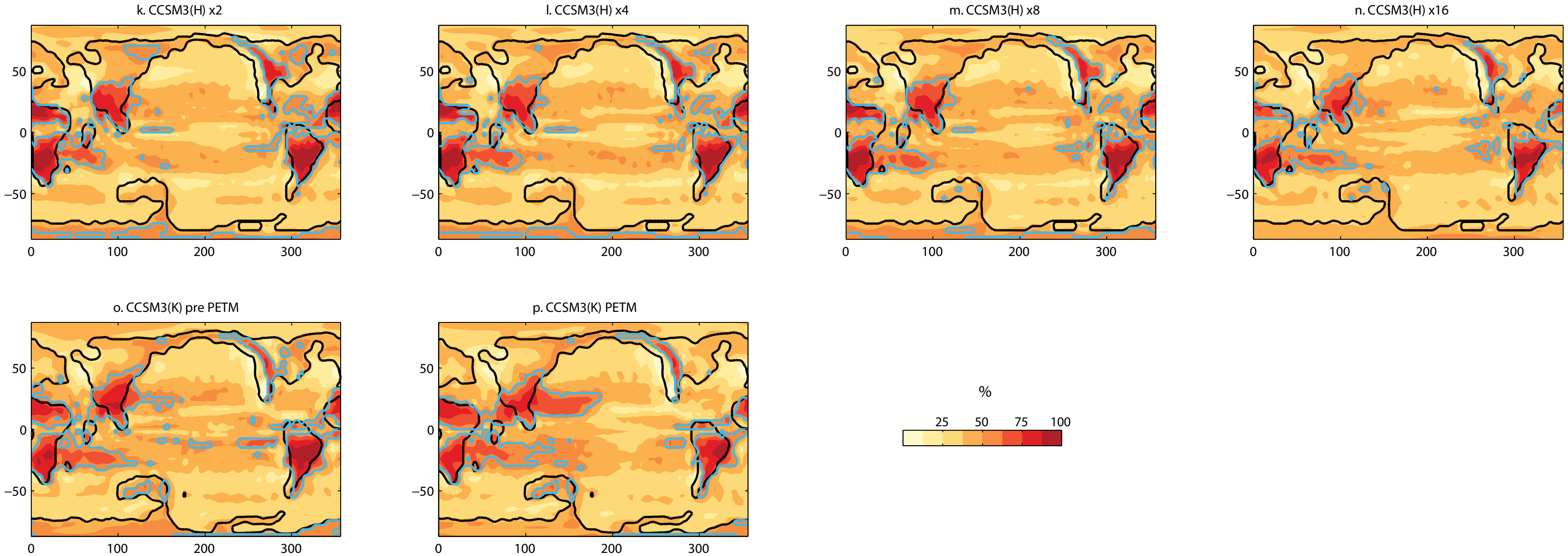
k. CCSM3(H) x2
l. CCSM3(H) x4
m. CCSM3(H) x8
n. CCSM3(H) x16
o. CCSM3(K) pre PETM
p. CCSM3(K) PETM
%
25
50
75
100

Figure 7b

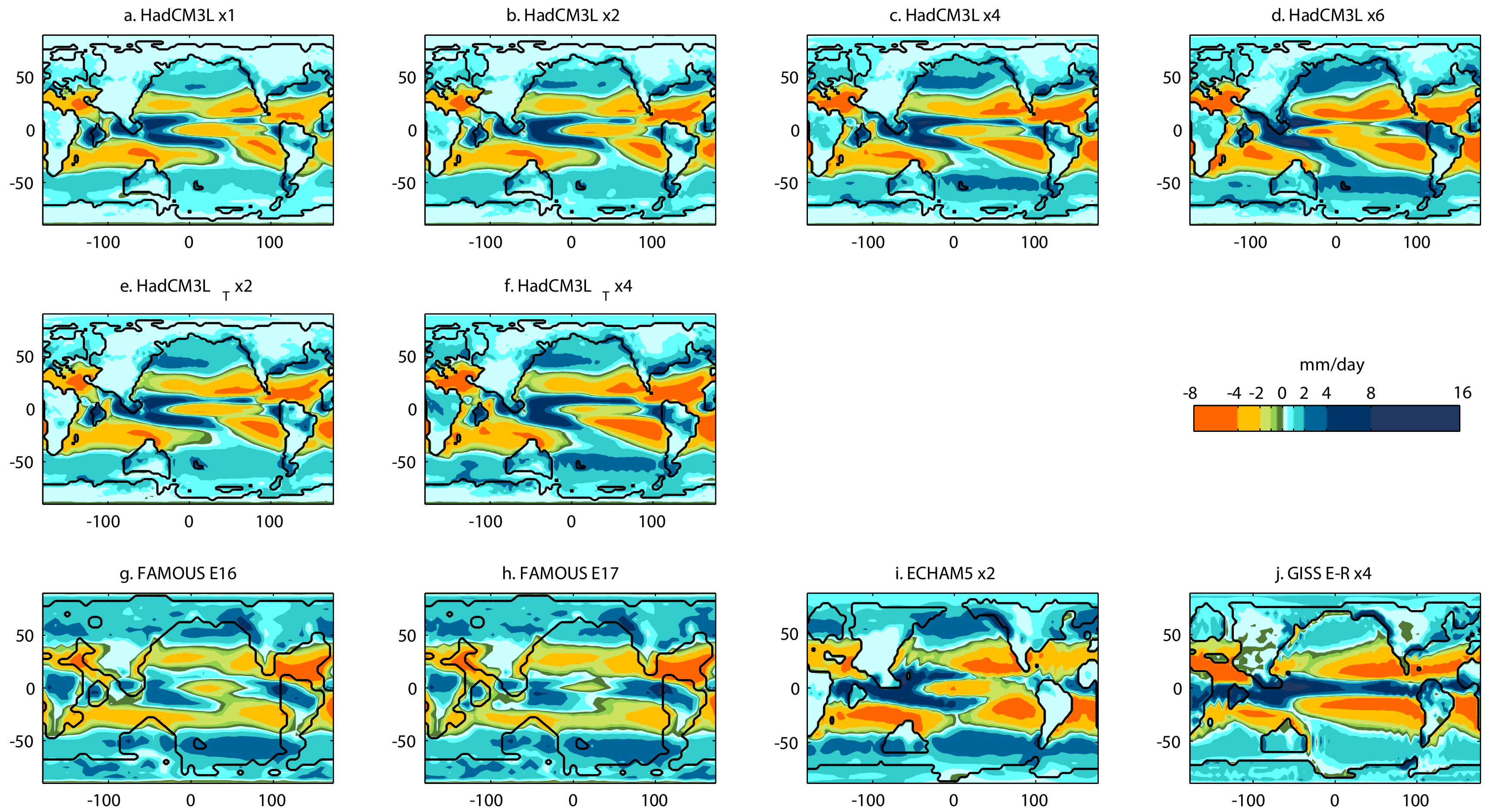
a. HadCM3L x1
b. HadCM3L x2
c. HadCM3L x4
d. HadCM3L x6
e. HadCM3L T x2
f. HadCM3L T x4
g. FAMOUS E16
h. FAMOUS E17
i. ECHAM5 x2
j. GISS E-R x4
mm/day
-8 -4 -2 0 2 4 8 16
50
0
-50
-100
0
100

Figure 8a

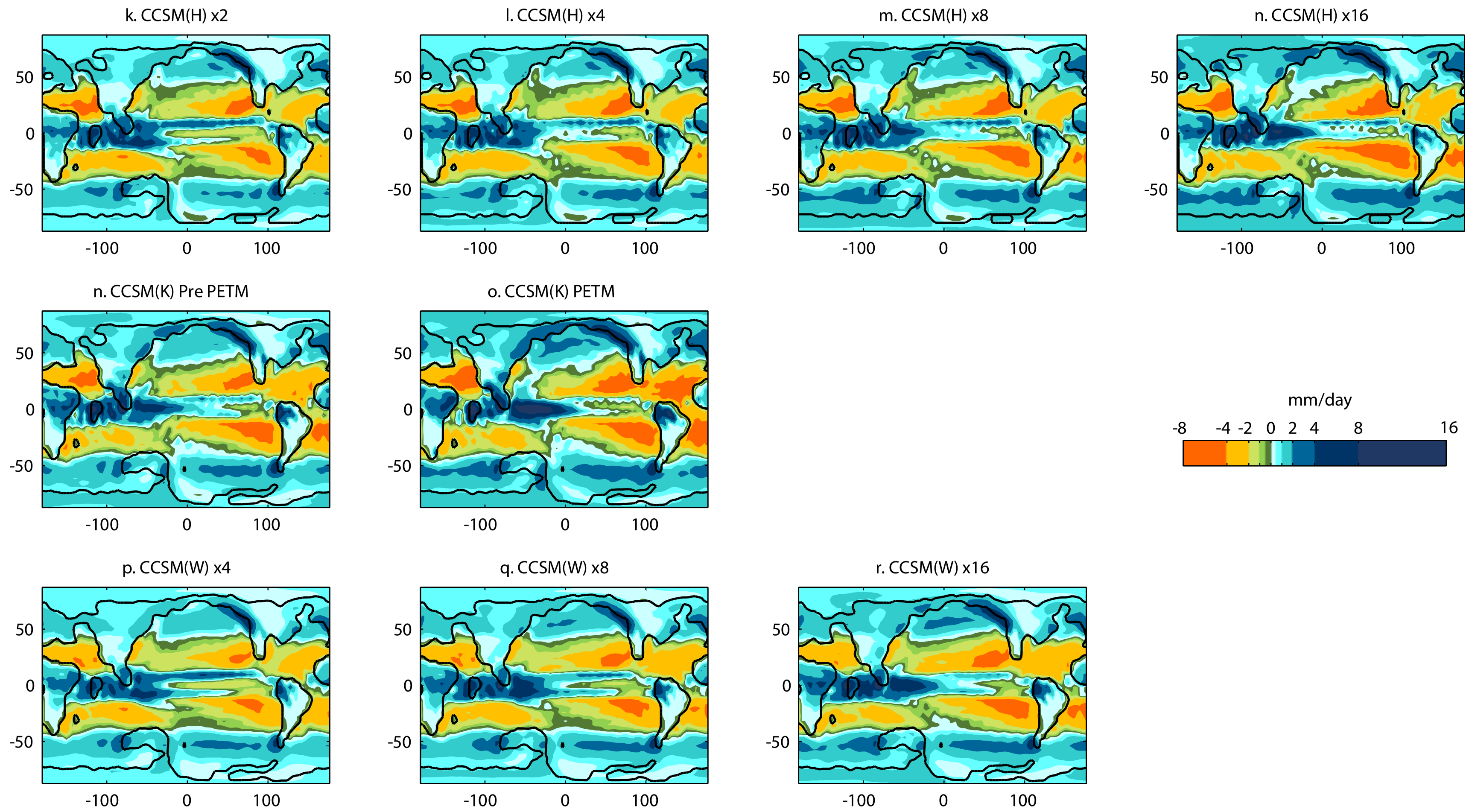
k. CCSM(H) x2
l. CCSM(H) x4
m. CCSM(H) x8
n. CCSM(H) x16
n. CCSM(K) Pre PETM
o. CCSM(K) PETM
p. CCSM(W) x4
q. CCSM(W) x8
r. CCSM(W) x16
mm/day
-8 -4 -2 0 2 4 8 16
50
0
-50
-100
0
100

Figure 8b

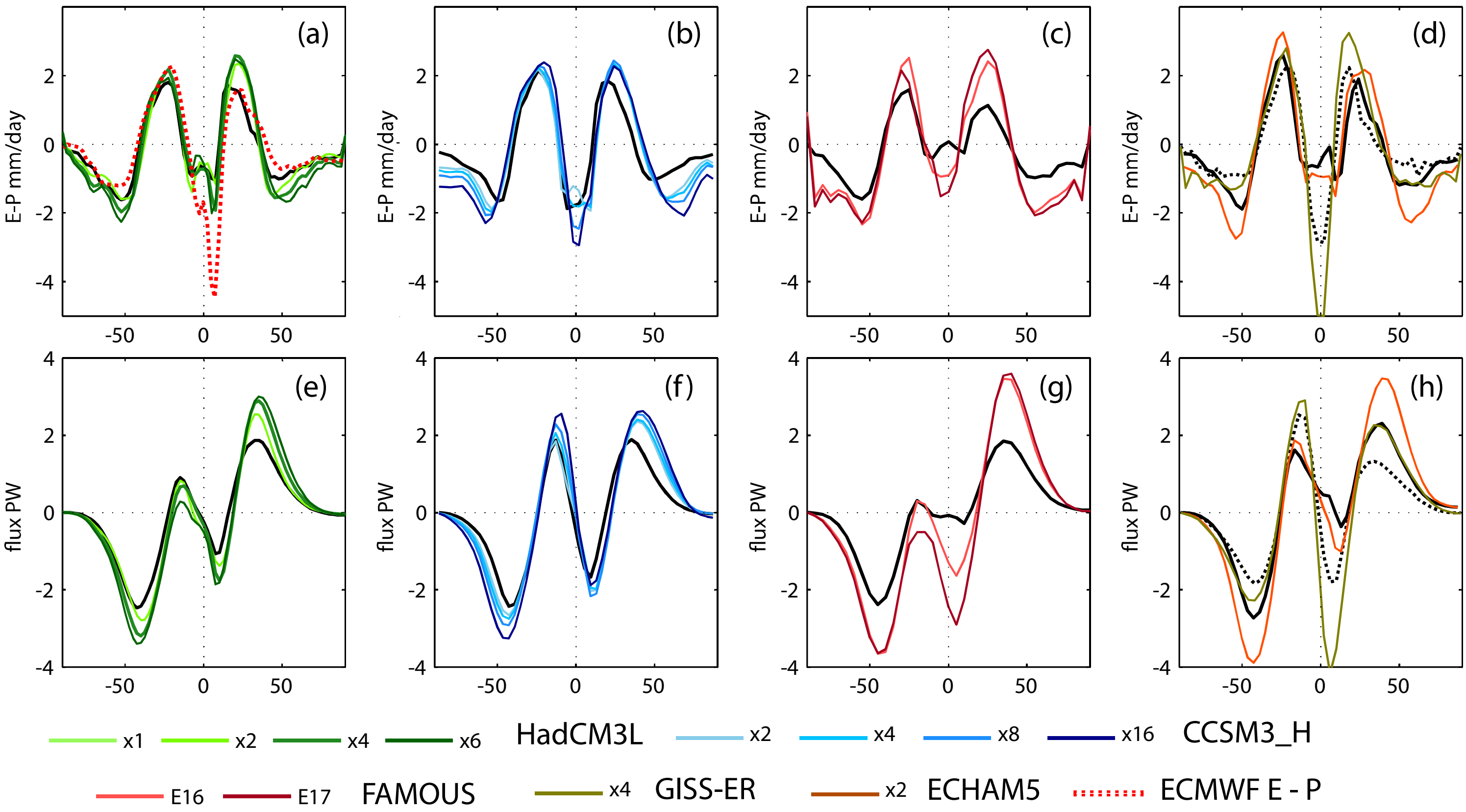
(a)
(b)
(c)
(d)
(e)
(f)
(g)
(h)
E-P mm/day
flux PW
x1
x2
x4
x6
HadCM3L
x2
x4
x8
x16
CCSM3_H
E16
E17
FAMOUS
x4
GISS-ER
x2
ECHAM5
ECMWF E - P

Figure 9

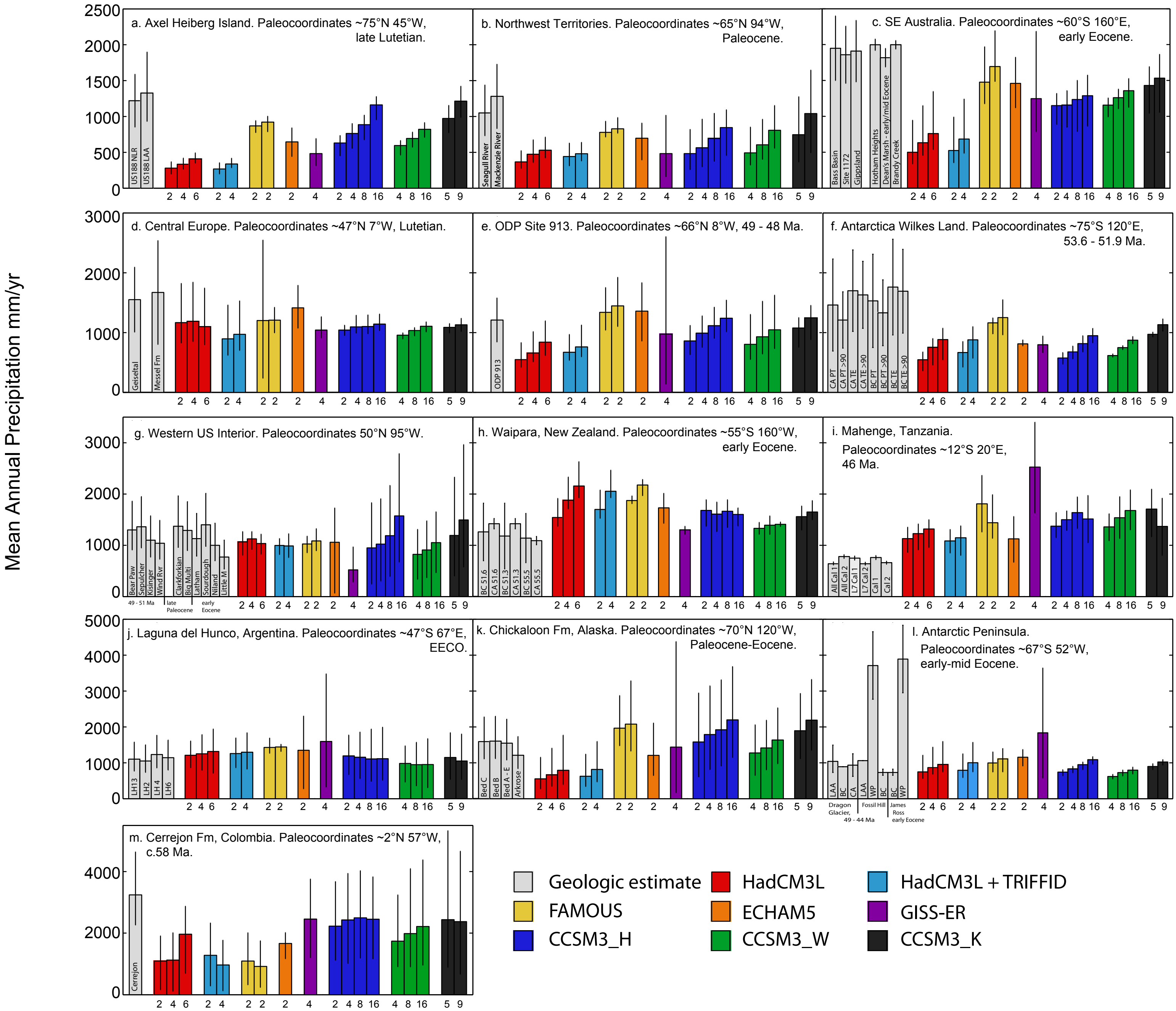

Mean Annual Precipitation mm/yr
a. Axel Heiberg Island. Paleocoordinates ~75°N 45°W, late Lutetian.
b. Northwest Territories. Paleocoordinates ~65°N 94°W, Paleocene.
c. SE Australia. Paleocoordinates ~60°S 160°E, early Eocene.
d. Central Europe. Paleocoordinates ~47°N 7°W, Lutetian.
e. ODP Site 913. Paleocoordinates ~66°N 8°W, 49 - 48 Ma.
f. Antarctica Wilkes Land. Paleocoordinates ~75°S 120°E, 53.6 - 51.9 Ma.
g. Western US Interior. Paleocoordinates 50°N 95°W.
h. Waipara, New Zealand. Paleocoordinates ~55°S 160°W, early Eocene.
i. Mahenge, Tanzania. Paleocoordinates ~12°S 20°E, 46 Ma.
j. Laguna del Hunco, Argentina. Paleocoordinates ~47°S 67°E, EECO.
k. Chickaloon Fm, Alaska. Paleocoordinates ~70°N 120°W, Paleocene-Eocene.
l. Antarctic Peninsula. Paleocoordinates ~67°S 52°W, early-mid Eocene.
m. Cerrejon Fm, Colombia. Paleocoordinates ~2°N 57°W, c.58 Ma.
Geologic estimate
HadCM3L
HadCM3L + TRIFFID
FAMOUS
ECHAM5
GISS-ER
CCSM3_H
CCSM3_W
CCSM3_K

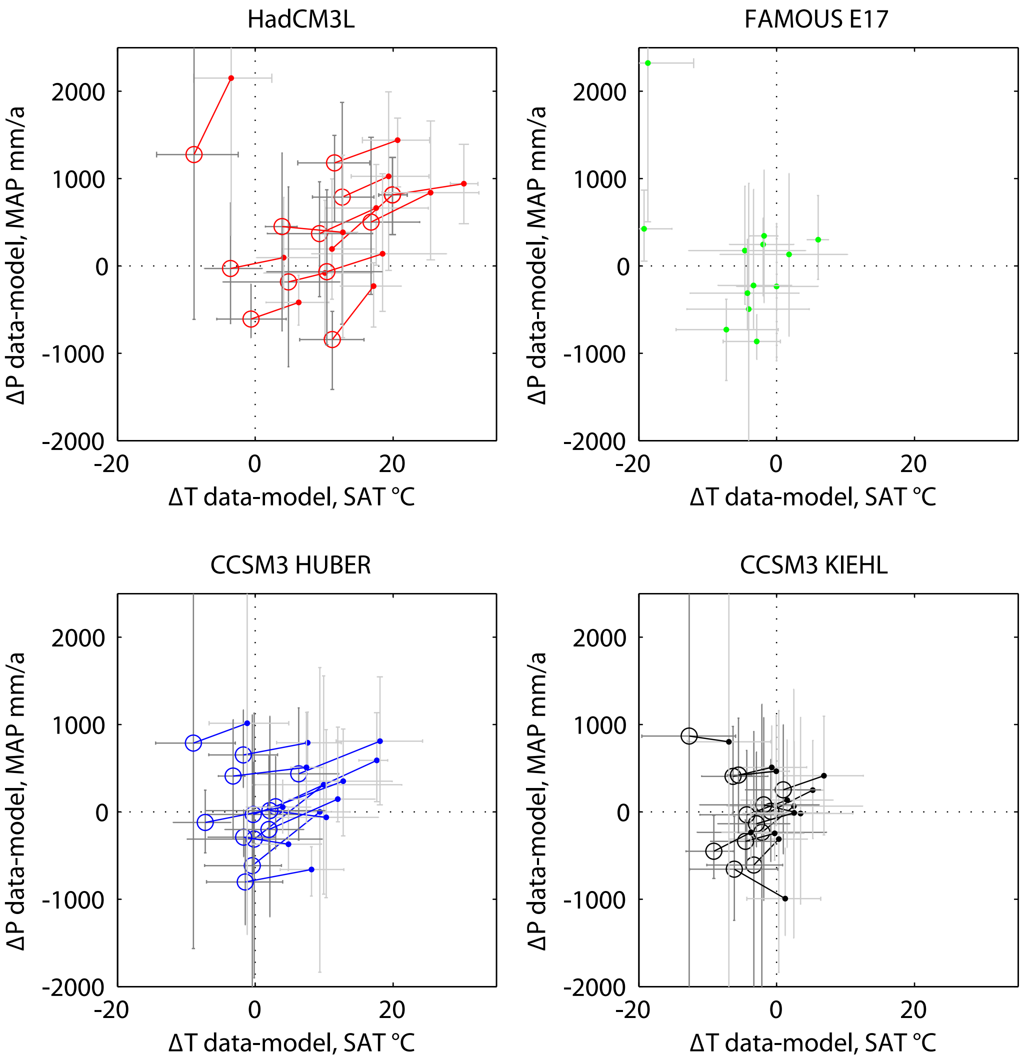

HadCM3L
FAMOUS E17
CCSM3 HUBER
CCSM3 KIEHL
ΔP data-model, MAP mm/a
ΔT data-model, SAT °C
2000
1000
0
-1000
-2000
-20
20

Figure 11

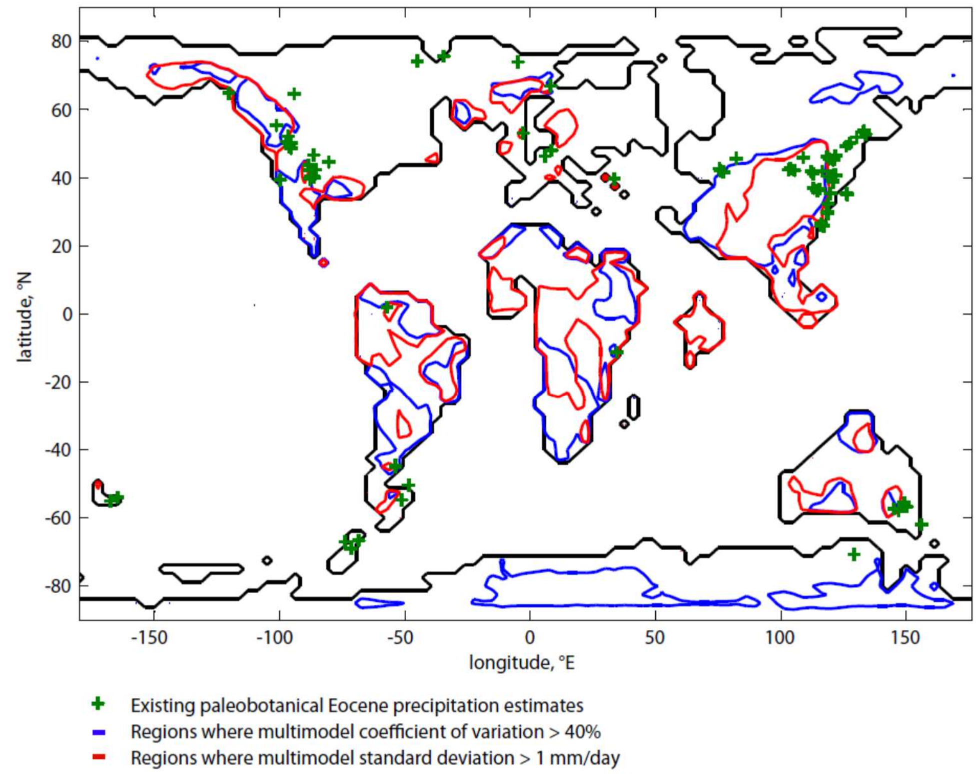

Figure 12 Summary of regions which show a significant model spread, based on the Eocene multimodel mean described in Figure 5. Paleobotanical estimates of quantitative precipitation rate included in the data compilation are shown by green markers. Regions where the standard deviation is greater than 1 mm/day are marked by a red outline and regions where the coefficient of variation (standard deviation/multimodel mean) is greater than 40% are outlined blue.

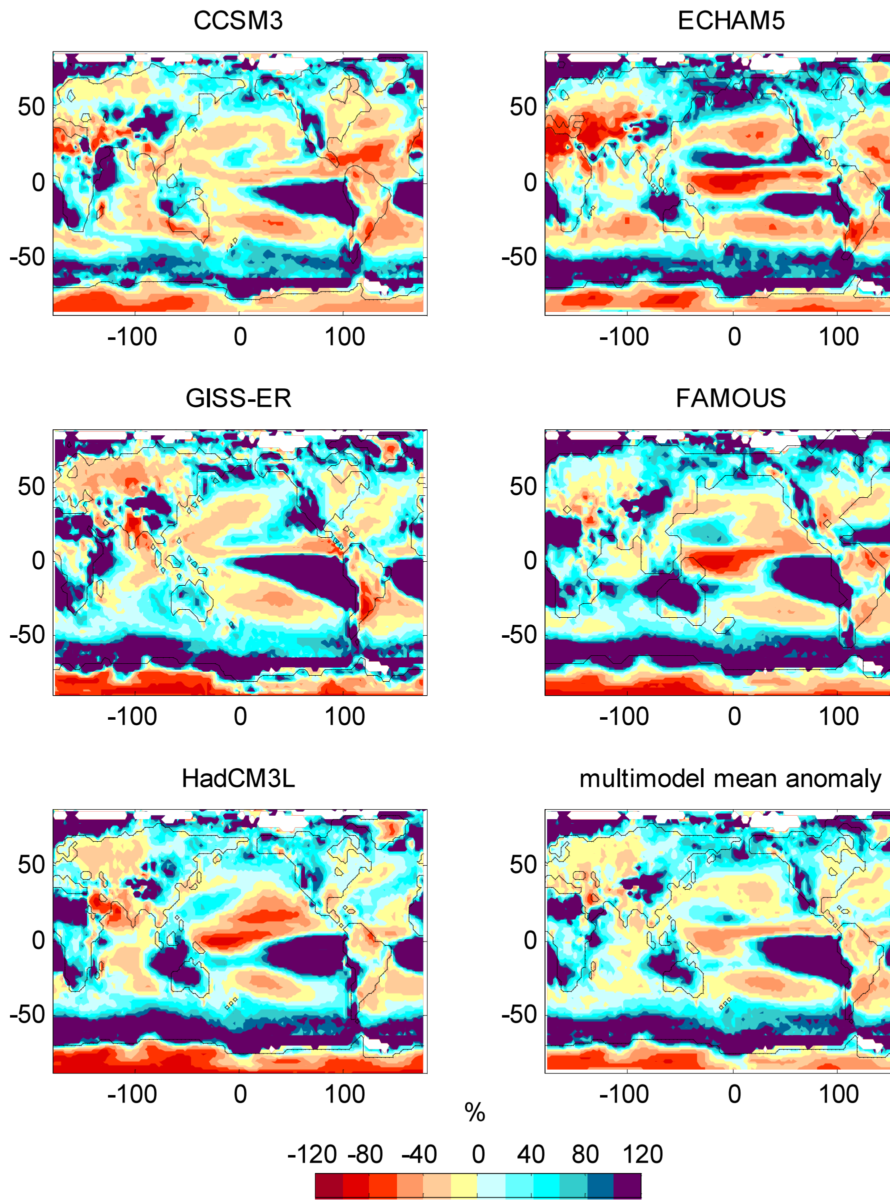
CCSM3
ECHAM5
GISS-ER
FAMOUS
HadCM3L
multimodel mean anomaly
50
0
-50
-100
0
100
%
-120 -80 -40 0 40 80 120

Figure S1

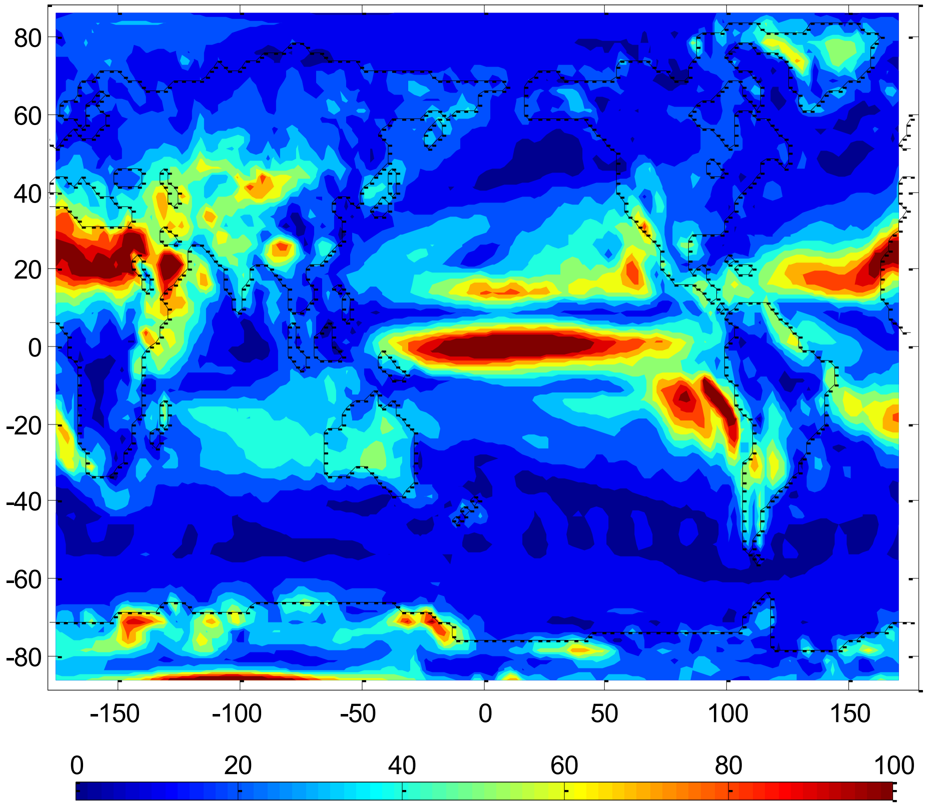

Figure S2

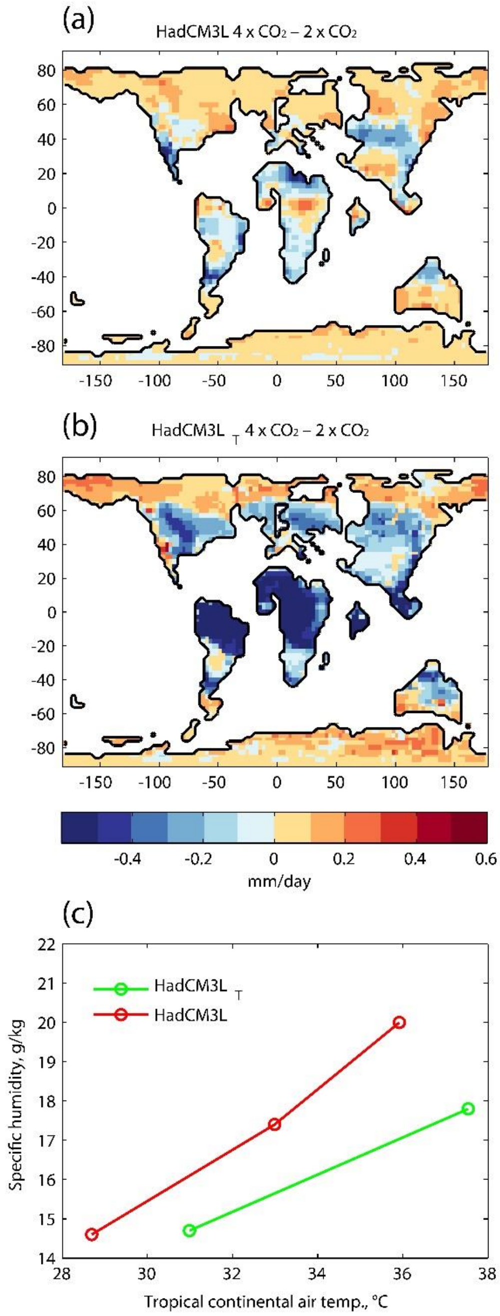

Figure S3 Changes in mean annual evapotranspiration 4 x CO_2 – 2 CO_2 simulations in HadCM3L in (a) the fixed shrubland simulations of Lunt et al. (2010) and (b) the TRIFFID dynamic vegetation simulations of Loptson et al. (2014). The differences in mean specific humidity relative to air temperature over tropical continents is shown in (c).

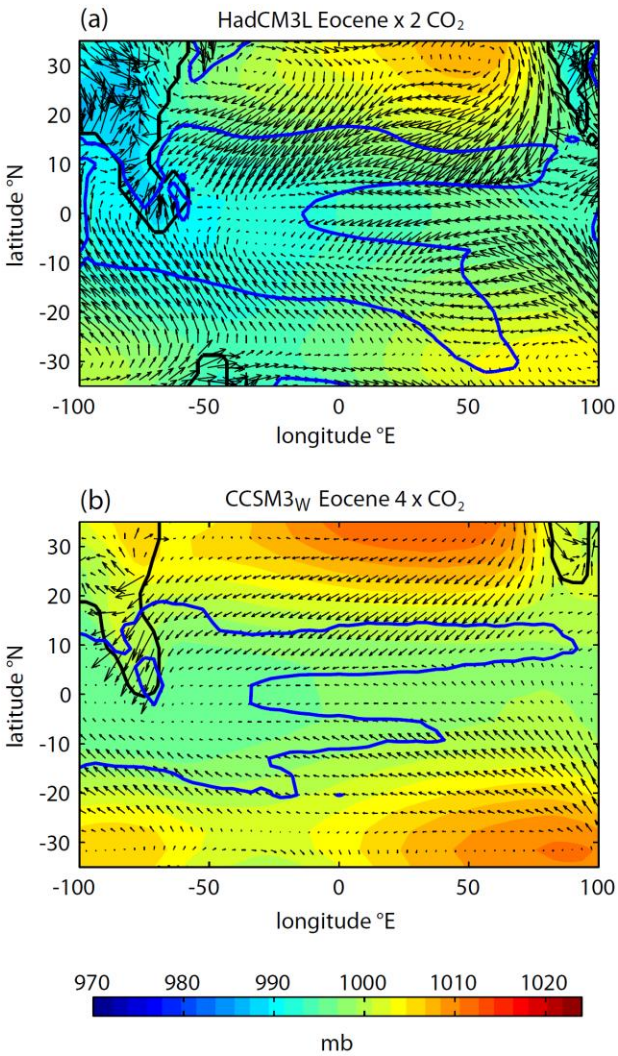

Figure S4 Surface pressure and winds over the South Pacific in Eocene simulations (a) HadCM3L, 2 x CO_2 and (b) CCSM3W, 4 x CO_2. The length of vectors is proportional to wind strength. The blue line shows the outline of the region where mean precipitation is greater than 5 mm/day.

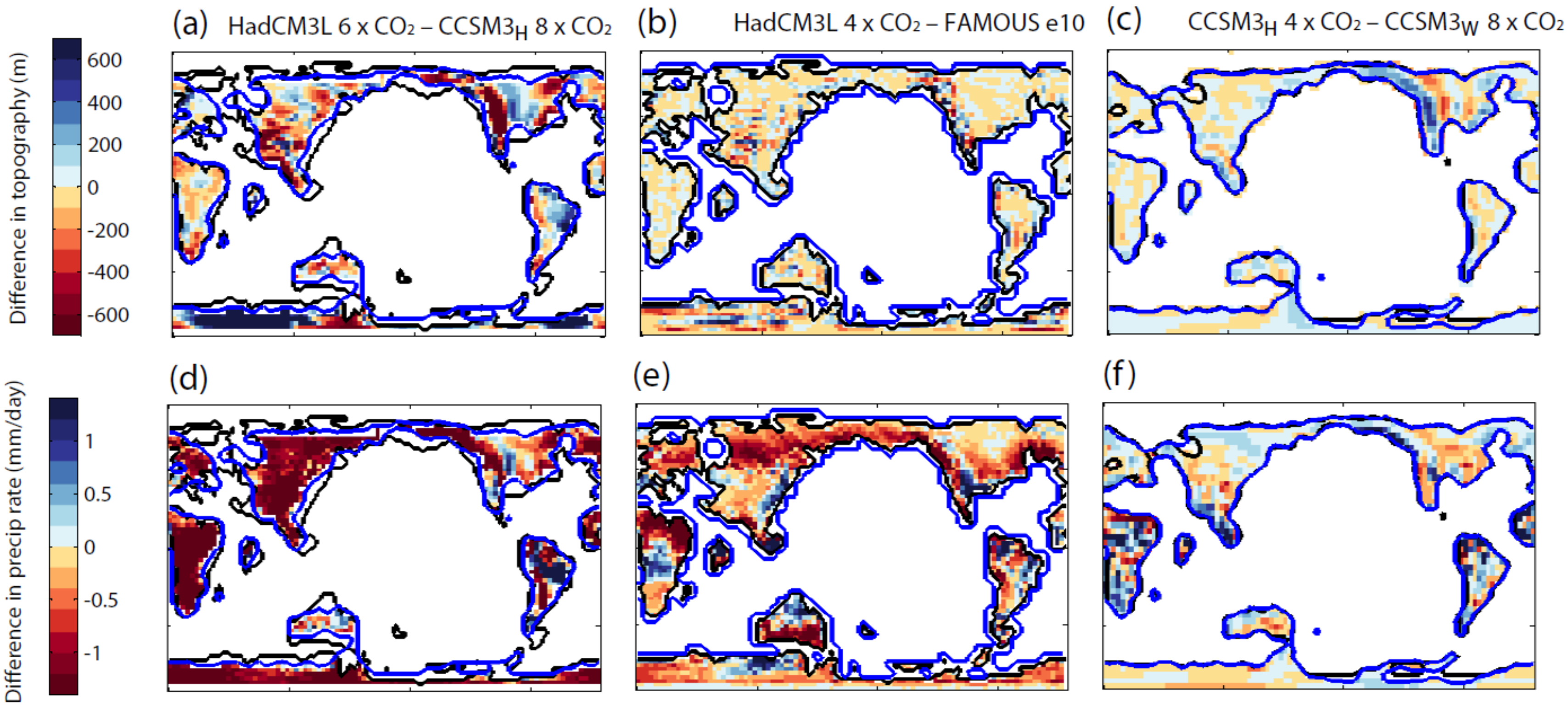

Figure S5 Differences in topography (a – c) and precipitation rate (d – f) in pairs of simulations; HadCM3L 6 x CO2 – CCSM3H 8 x CO2 (a,d); HadCM3L 4 x CO2 – FAMOUS e10 (b,e) and CCSM3H 4 x CO2 and CCSM3W 8xCO2. Simulations are chosen which have similar global precipitation rates (Figure 2).

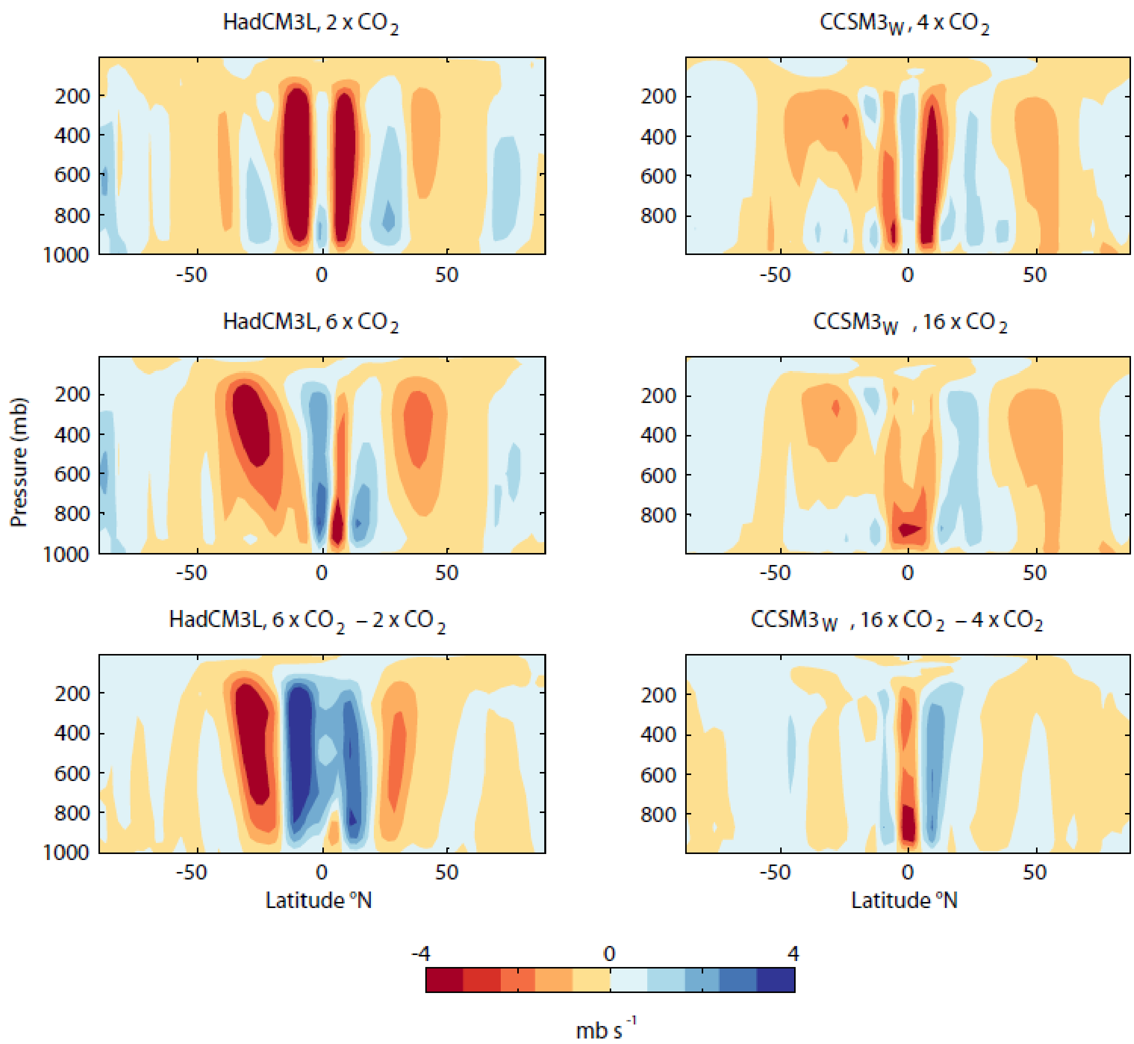

Figure S6 Vertical velocity of atmosphere averaged over 150°E to 150°W for HadCM3L simulations (left) and CCSM3(W) simulations (right). The bottom figures shows anomalies for the high CO_2 – low CO_2 simulations.

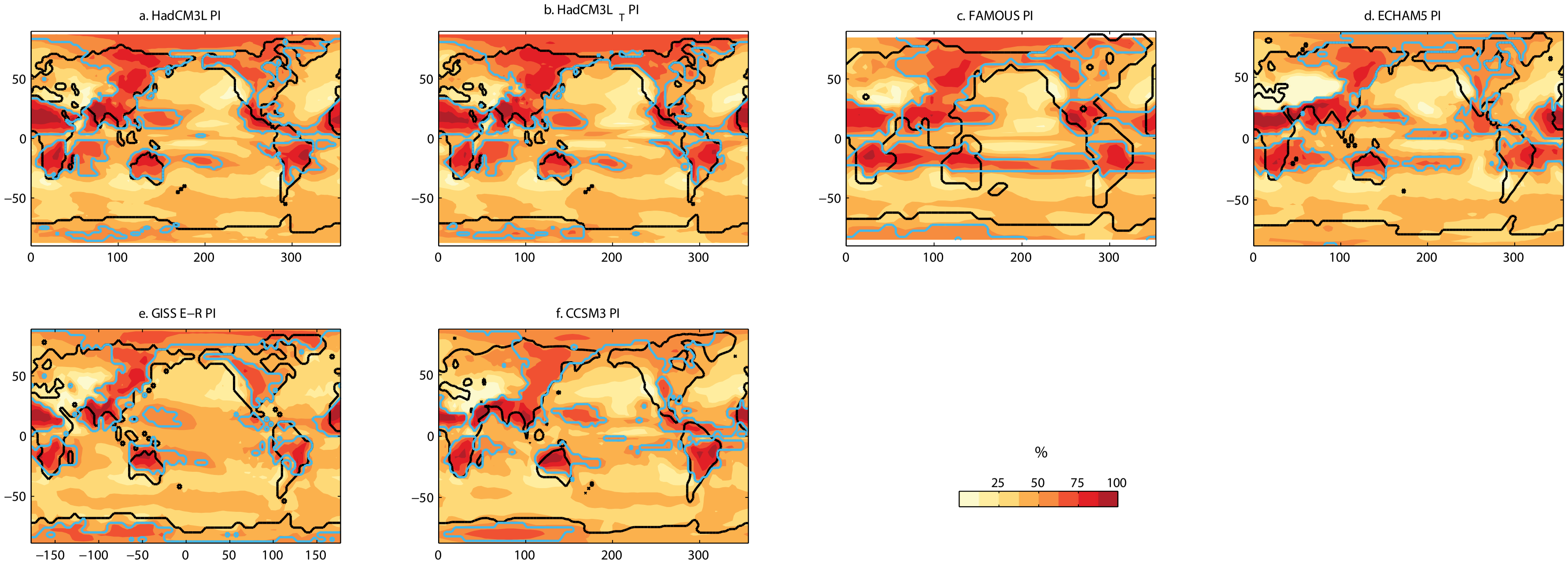
a. HadCM3L PI
b. HadCM3L T PI
c. FAMOUS PI
d. ECHAM5 PI
e. GISS E−R PI
f. CCSM3 PI
%
25
50
75
100
50
0
−50
0
100
200
300
−150
−100
−50
0
50
100
150

Figure S7

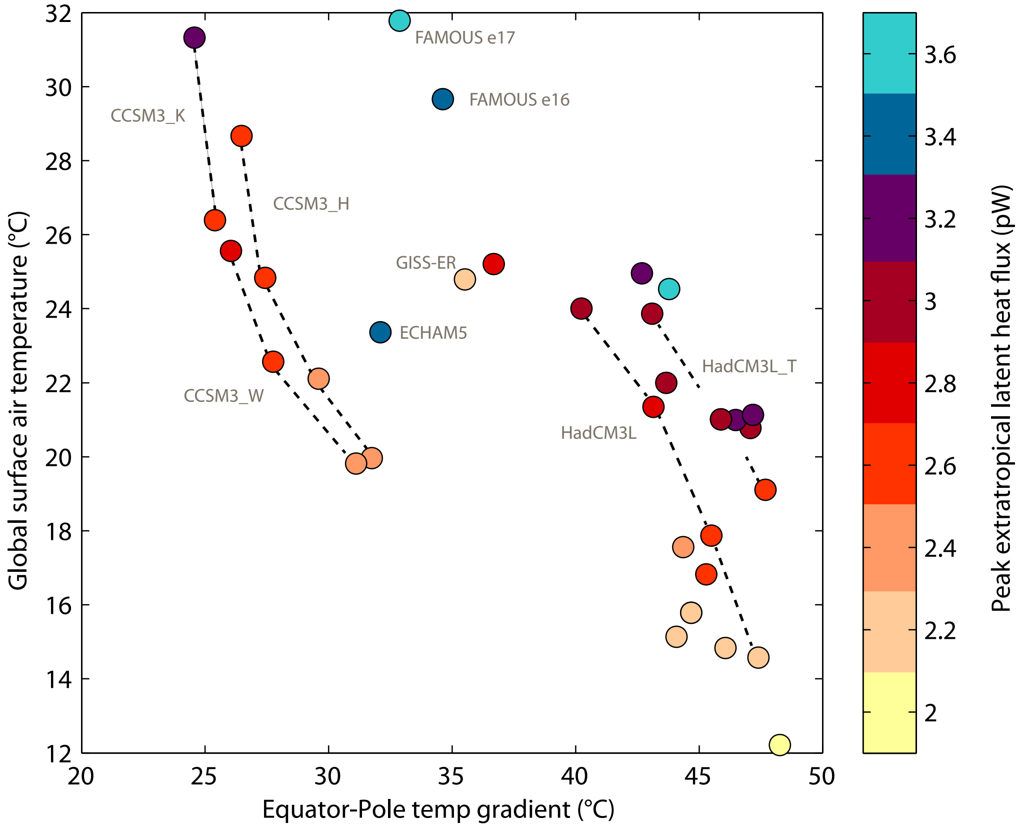

Global surface air temperature (°C)
Equator-Pole temp gradient (°C)
Peak extratropical latent heat flux (pW)
FAMOUS e17
FAMOUS e16
CCSM3_K
CCSM3_H
GISS-ER
ECHAM5
CCSM3_W
HadCM3L_T
HadCM3L

Figure S9

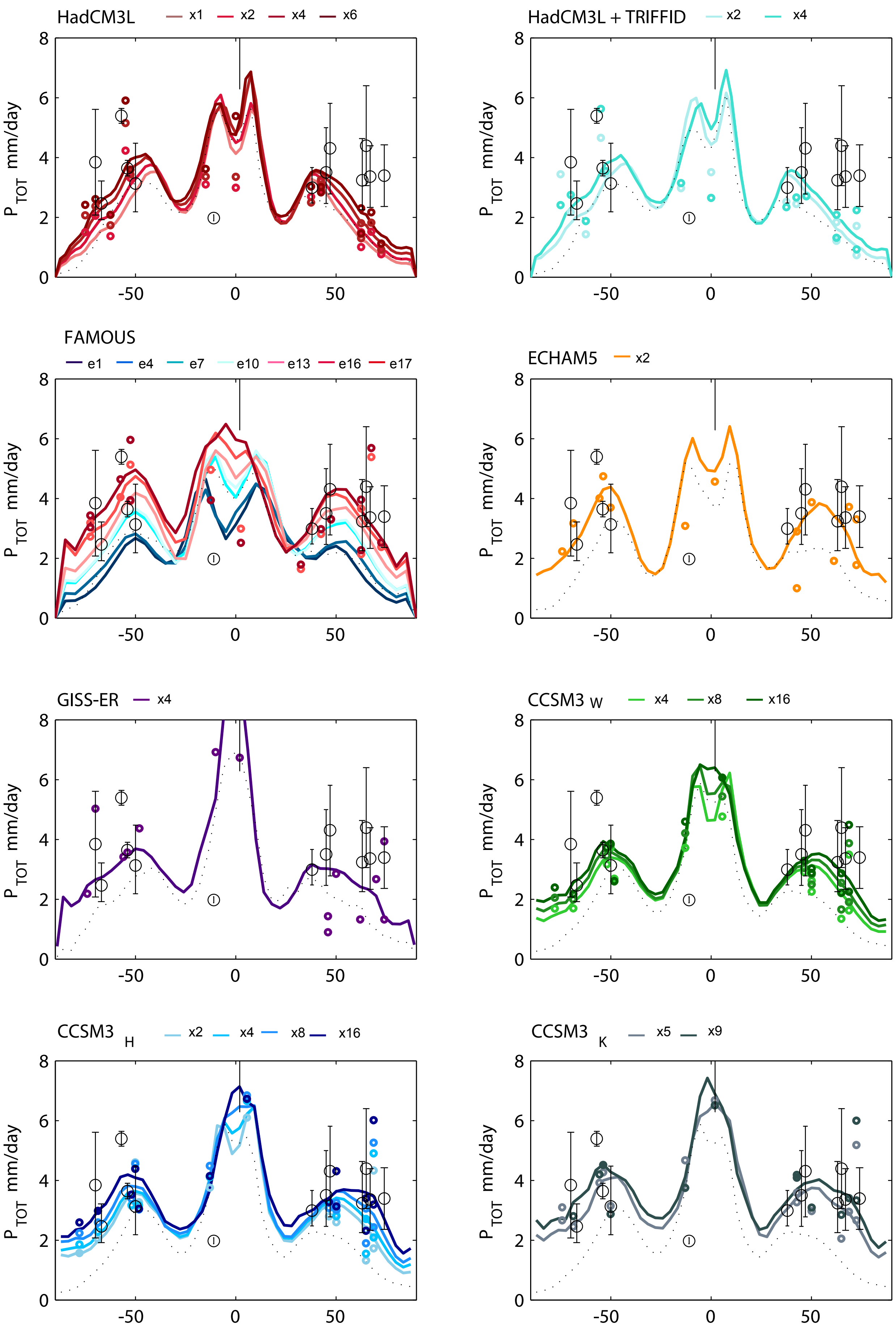

HadCM3L
x1
x2
x4
x6
HadCM3L + TRIFFID
x2
x4
FAMOUS
e1
e4
e7
e10
e13
e16
e17
ECHAM5
x2
GISS-ER
x4
CCSM3 W
x4
x8
x16
CCSM3 H
x2
x4
x8
x16
CCSM3 K
x5
x9
P TOT mm/day
0
2
4
6
8
-50
0
50

Model	Eocene simulation reference	Model reference	Atmosphere resolution	Ocean resolution	Paleogeography	Sim. length (years)	CO_2 levels	Orbital configuration
HadCM3L HadCM3L (T)	Lunt et al. (2010) Loptson et al. (2014)	Cox et al. (2001)	96 x 73 x 19	96 x 73 x 20	Proprietary	> 3400	x 1,2,4,6 x 2,4	Preindustrial orbit.
ECHAM5	Heinemann et al. (2009)	Roeckner et al. (2003)	96 x 48 x 19	142 x 82 x 40	Bice and Marotzke (2001)	2500	x 2	*e* = 0.0300; *o* = 23.25; *p* = 270
CCSM3 (W)	Winguth et al. (2010, 2012)	Collins et al. (2006); Yeager et al. (2006)	96 x 48 x 26	100 x 116 x 25	Sewall et al. (2000) with marginal sea parameterisation	1500	x 4,8,16	*e = 0; o* = 23.5;
CCSM3 (H)	Liu et al. (2009); Huber and Caballero (2011)	Collins et al. (2006); Yeager et al. (2006)	96 x 48 x 26	100 x 122 x 25	Sewall et al. (2000)	1500	x2,4,8,16	Preindustrial orbit.
CCSM3 (K)	Kiehl and Shields (2013)	Collins et al. (2006); Yeager et al. (2006)	96 x 48 x 26	100 x 116 x 25	As CCSM(W)	>2000 > 3600 +	x~5 x ~9	As CCSM(W)
GISS E-R	Roberts et al. (2009)	Schmidt et al. (2006)	72 x 45 x 20	72 x 45 x 13	Bice and Marotzke (2001)	2000	x ~4	*e* = 0.0270; *o* = 23.20, *p* = 180
FAMOUS	Sagoo et al. (2013)	Jones et al. (2005), Smith et al. (2008).	48 x 37 x 11	96 x 73 x 20	Proprietary	> 1500	x 2	Preindustrial orbit.

Model	Stratiform precipitation	Convective precipitation	Vegetation	Aerosols
HadCM3	Large-scale precipitation is calculated based on cloud water and ice contents (similar to Smith, 1990)	Bulk mass flux scheme (Gregory and Rowntree, 1990), with improvement by Gregory et al. (1997)	Homogenous shrubland (Lunt) Dynamically evolving vegetation TRIFFID (Loptson)	As control
ECHAM5	Prognostic equations for the water phases, bulk cloud microphysics (Lohmann and Roeckner, 1996)	Bulk mass flux scheme (Tiedtke 1989) with modifications for deep convection according to Nordeng (1994).	Homogenous woody savannah	As control
CCSM_W	Prognostic condensate and precipitation parameterisation (Zhang et al., 2003)	Simplified Arakawa and Schubert (1974) (cumulus ensemble) scheme developed by Zhang and McFarlane (1995)	Shellito and Sloan (2006)	As control
CCSM_H			Sewall et al. (2000)	Reduced aerosol loading.
CCSM_K			Sewall et al. (2000)	Cloud microphysical parameters altered.
GISS E-R	Prognostic stratiform cloud based on moisture convergence (Del Genio et al. 1996)	Bulk mass flux scheme by Del Genio and Yao (1993)	Sewall et al. (2000)	As control
FAMOUS	Precipitation parameterisation schemes are based on those of HadCM3.		Homogenous shrubland.	Uncertain perturbed parameters include those relating to cloud microphysical properties.

Table 1 Summary of model simulations in the ensemble adapted from Table 1 of Lunt et al. (2012). Additions detailing precipitation schemes are from Table 2 of Dai (2006). Some models have irregular grids in the atmosphere and/or ocean, or have spectral atmospheres. The atmospheric and ocean resolution are given in number of gridboxes, X x Y x Z where X is the effective number of gridboxes in the zonal, Y in the meridional, and Z in the vertical. *e* = eccentricity; *o* = obliquity; *p* = longitude of perihelion.

Model simulations	**P-T regression***	**% increase P per °C warming over range****
HadCM3L	P=0.0542T+2.1747	1.81
HadCM3L(T)	P=0.0398T+2.4278	1.32
CCSM3_H	P=0.0594T+2.0506	2.02
CCSM3_K	P=0.0628T+1.9739	2.15
CCSM3_W	P=0.0596T+1.9341	2.11
FAMOUS	P=0.0774T+1.6006	2.80

Table 2 Summary of relationships between global Surface Air Temperature and precipitation rate. *T = SAT °C, P = global precipitation mm/day.
** Precipitation sensitivity is calculated over the range of 15 – 30°C.

Model	PI	x1 CO_2	x2 CO_2	x4/5 CO_2	x6/8/9 CO_2	x16 CO_2
HadCM3L	60.1	66.3	62.6	57.7	52.3	
HadCM3L(T)			62.0	51.6		
ECHAM5	50.1		41.6			
GISS E-R	47.7			37.6		
CCSM(H)	50.1		47.3	44.2	42.4	35.1
CCSM(K)				47.5	34.12	
FAMOUS	48.9		28.1 E16 23.6 E17			

Table 3 % land surface characterised by extended summer precipitation > 55% MAP

Simulation	Global mean precipitation (mm day^{-1})	Global mean evaporation (mm day^{-1})	Residual water mass (x 10^{12} kg)	Latent heat forcing (x 10^{13} W)
HadCM3L				
Preindustrial	2.915	2.910	2.565	6.710
Eocene x1	3.007	3.005	1.254	3.279
Eocene x2	3.202	3.199	1.380	3.610
Eocene x4	3.376	3.372	1.707	4.465
Eocene x6	3.510	3.507	1.878	4.916
Preindustrial TRIFFID	2.866	2.866	0.2212	0.5786
Eocene x2 TRIFFID	3.233	3.233	0.1615	0.4225
Eocene x4 TRIFFID	3.415	3.415	0.1819	0.4758
ECHAM5				
Preindustrial	2.749	2.759	-5.154	-13.48
Eocene x2	3.423	3.433	-5.264	-13.77
GISS-ER				
Preindustrial	2.968	2.966	0.5774	1.510
Eocene x4	3.675	3.673	1.077	2.816
FAMOUS				
Preindustrial	2.908	2.912	-2.361	-6.176
E16	3.936	9.939	-1.545	-4.042
E17	4.135	4.137	-1.245	-3.255
CCSM3				
Preindustrial	2.650	2.648	1.164	3.044
Eocene H x2	3.288	3.285	1.082	2.830
Eocene H x4	3.415	3.413	1.121	2.932
Eocene Hx8	3.572	3.570	1.208	3.159
Eocene Hx16	3.790	3.780	5.062	13.24
Eocene Wx4	3.168	3.166	1.080	2.824
Eocene Wx8	3.332	3.330	1.166	3.049
Eocene Wx16	3.499	3.496	1.248	3.263
Eocene Kx5	3.678	3.677	1.321	3.455
Eocene Kx9	3.969	3.966	1.640	4.290

Table S1 Assessment of the imbalance between global precipitation and evaporation rates in the EoMIP ensemble. The imbalance is additionally shown as a global residual water mass and equivalent latent heat forcing.

	Preindustrial						Eo x 1 CO2	Eocene x 2 CO2					Eocene x 4 CO2					Eo x ~5 CO2	Eo x 6 CO2	Eocene x 8 CO2		Eo x ~9 CO2	Eocene x 16 CO2	
	HadCM	HadCM TRIFFID	FAMOUS	CCSM *	ECHAM	GISS	HadCM	HadCM	HadCM	FAMOUS E17	ECHAM	CCSM H	HadCM	HadCM	CCSM H	CCSM W	GISS	CCSM K	HadCM	CCSM H	CCSM W	CCSM K	CCSM H	CCSM W
GL P_{TOT}	2.91	2.87	2.91	2.65	2.75	2.97	3.01	3.20	3.23	4.13	3.42	3.29	3.38	3.42	3.42	3.17	3.67	3.68	3.51	3.57	3.33	3.97	3.79	3.50
GL P_{CV}		2.16	2.37	1.99	1.80		2.38	2.56	2.60	3.75	2.37	2.65	2.73	2.80	2.78	2.57		3.12	2.89	2.96	2.76	3.39	3.19	2.93
GL P_{LS}		0.71	0.54	0.66	0.95		0.63	0.64	0.63	0.39	1.05	0.63	0.64	0.62	0.63	0.60		0.56	0.62	0.61	0.58	0.58	0.60	0.57
GL P_{CV}/P_{TOT}		0.75	0.81	0.75	0.65		0.79	0.80	0.80	0.91	0.69	0.81	0.81	0.82	0.81	0.81		0.85	0.82	0.83	0.83	0.85	0.84	0.84
GL Temp /°C	12.72	11.87	14.36	11.62	13.54	13.79	14.57	17.87	19.11	31.77	23.36	19.96	21.35	23.86	22.10	19.82	24.79	26.39	24.00	24.83	22.56	31.32	28.67	25.56
LA P_{TOT}	2.14	2.20	2.62	1.90	1.81	2.45	2.08	2.25	2.29	3.22	2.57	3.11	2.40	2.36	3.36	2.90	3.12	3.66	2.65	3.61	3.18	3.93	3.86	3.43
LA P_{CV}		1.66	2.17	1.40	1.05		1.59	1.71	1.77	2.63	1.37	2.37	1.84	1.80	2.61	2.26		2.98	2.07	2.85	2.52	3.23	3.10	2.76
LA P_{LS}		0.54	0.44	0.50	0.76		0.49	0.54	0.52	0.60	1.21	0.74	0.56	0.55	0.75	0.64		0.69	0.58	0.76	0.66	0.70	0.76	0.67
LA P_{CV}/P_{TOT}		0.75	0.83	0.74	0.58		0.76	0.76	0.77	0.82	0.53	0.76	0.77	0.76	0.78	0.78		0.81	0.78	0.79	0.79	0.82	0.80	0.80
LA Temp /°C	6.26	5.65	10.64	6.18	7.70	8.19	8.05	12.07	14.64	30.01	20.90	16.24	16.54	21.03	18.93	16.71	21.98	24.65	20.14	22.17	19.99	30.68	26.85	23.59
OC P_{TOT}	3.23	3.14	3.12	2.96	3.12	3.18	3.38	3.59	3.62	4.80	3.74	3.35	3.77	3.85	3.43	3.26	3.87	3.68	3.86	3.56	3.38	3.98	3.77	3.52
OC P_{CV}		2.36	2.52	2.23	2.10		2.70	2.90	2.94	4.58	2.75	2.75	3.09	3.21	2.85	2.68		3.17	3.23	2.99	2.83	3.44	3.22	2.99
OC P_{LS}		0.76	0.61	0.73	1.02		0.68	0.69	0.68	0.23	0.99	0.60	0.68	0.64	0.59	0.58		0.52	0.63	0.57	0.55	0.54	0.55	0.53
OC P_{CV}/P_{TOT}		0.75	0.81	0.75	0.67		0.80	0.81	0.81	0.95	0.74	0.82	0.82	0.83	0.83	0.82		0.86	0.84	0.84	0.84	0.86	0.85	0.85
LA/OC P_{TOT}	0.66	0.70	0.84	0.64	0.58	0.77	0.62	0.63	0.63	0.67	0.69	0.93	0.64	0.61	0.98	0.89	0.81	0.99	0.69	1.01	0.94	0.99	1.02	0.97
OC Temp /°C	15.35	14.41	17.14	13.88	15.88	16.12	17.23	20.23	20.92	33.08	24.29	21.21	23.30	25.02	23.17	20.86	25.91	26.96	25.58	25.72	23.43	30.68	26.85	23.59

Table S2 Sensitivity of the global Eocene hydrological cycle. Rates shown represent annual mean precipitation mm day^{-1}. GL = globally averaged rate; LA = land surface rate; OC = sea surface rate. TOT = total precipitation rate; CV = convective precipitation; LS = large-scale precipitation. Note that CV and LS sum to give total precipitation rate, but land and ocean represent averages over those regions.

* CCSM_W, CCSM_H and CCSM_K share a preindustrial simulation.